Stellar Magnetism and Space Weather in Exo-Planetary Systems

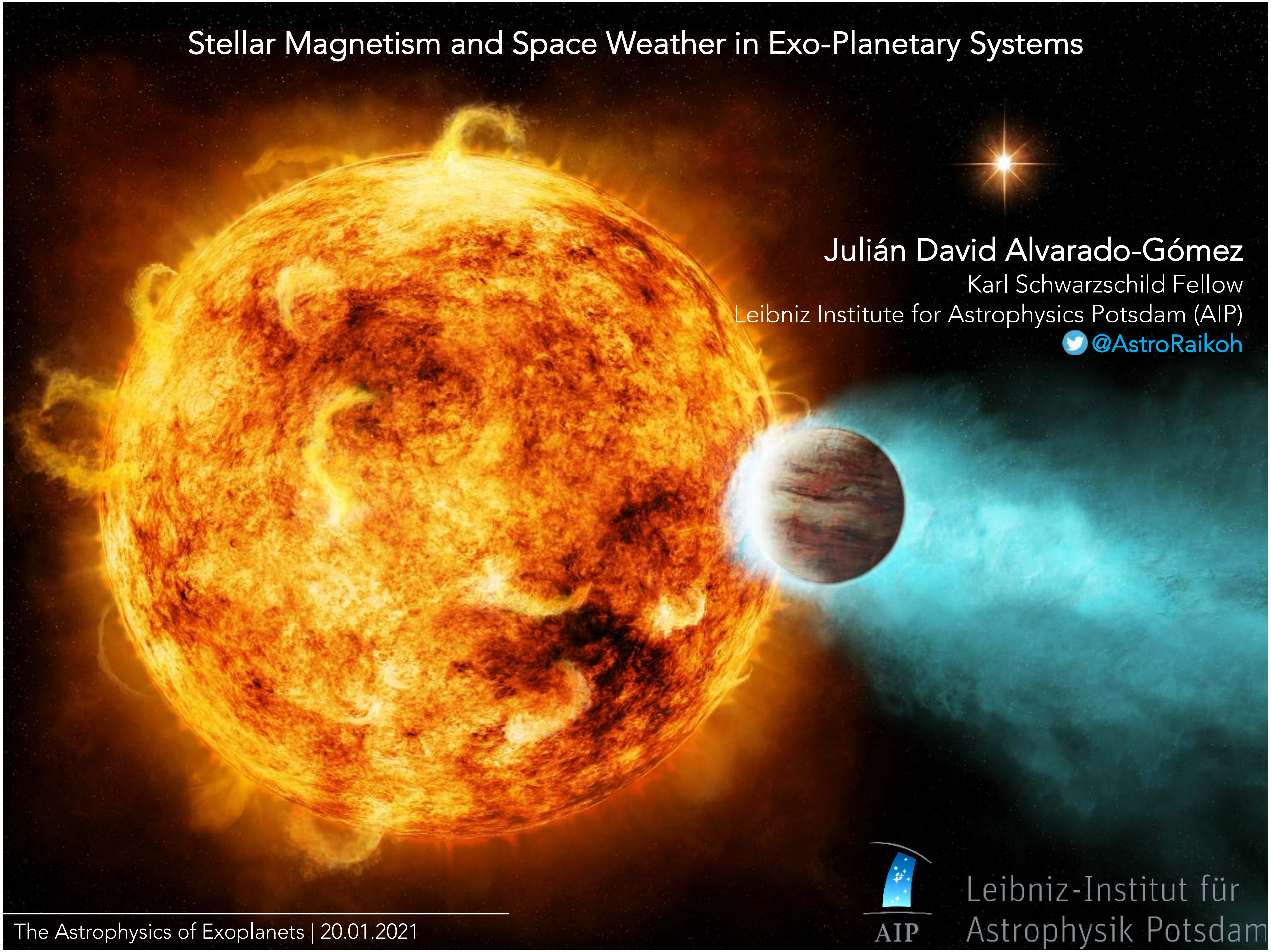

Julián David Alvarado-Gómez
Karl Schwarzschild Fellow
Leibniz Institute for Astrophysics Potsdam (AIP)
@AstroRaikoh

AIP
Leibniz-Institut für Astrophysik Potsdam

Motivation: Understand the effects of stellar magnetic fields on the surrounding environment

High-Energy Emission

Coronal Structure + Stellar Wind + Planetary Conditions

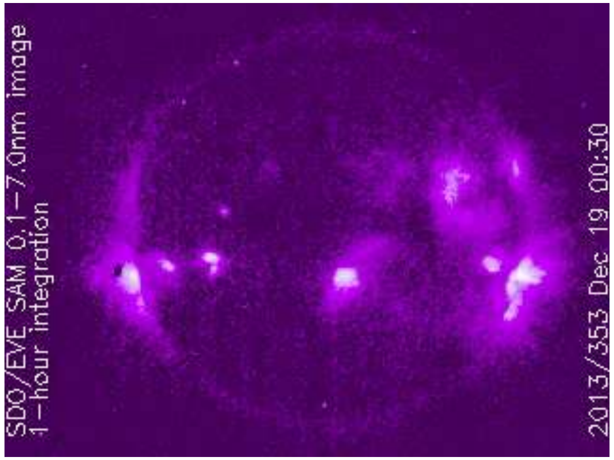

Transient Phenomena (Flares/CMEs)

Astrospheres

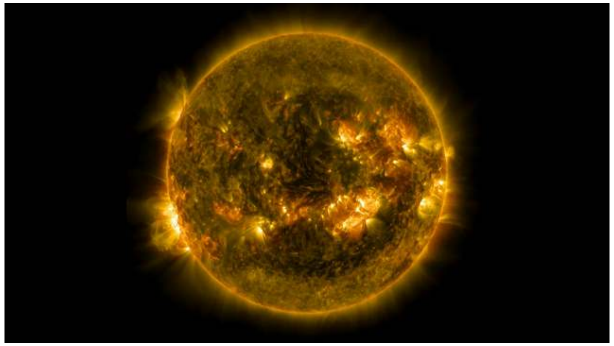

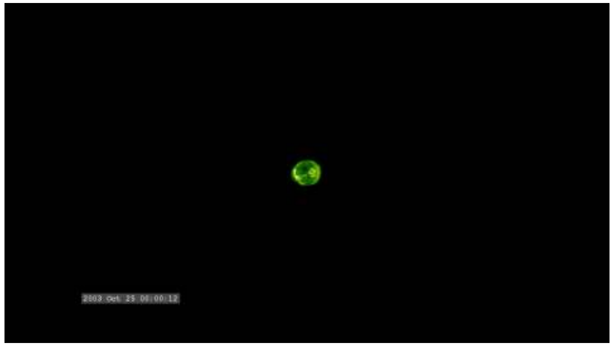

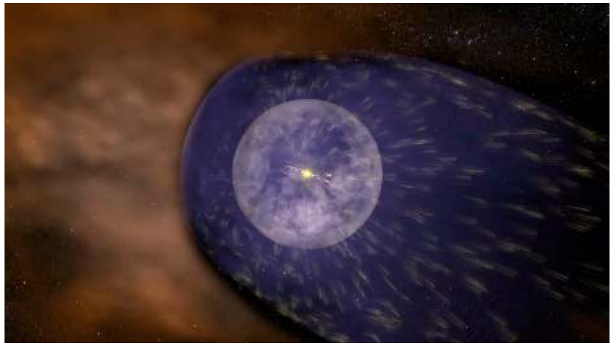

NASA Goddard (SVS)

Advanced Observational Techniques ⟷ Detailed Numerical Simulations

Motivation: Understand the effects of stellar magnetic fields on the surrounding environment

The Habitable Zone (HZ) of low-mass main sequence stars

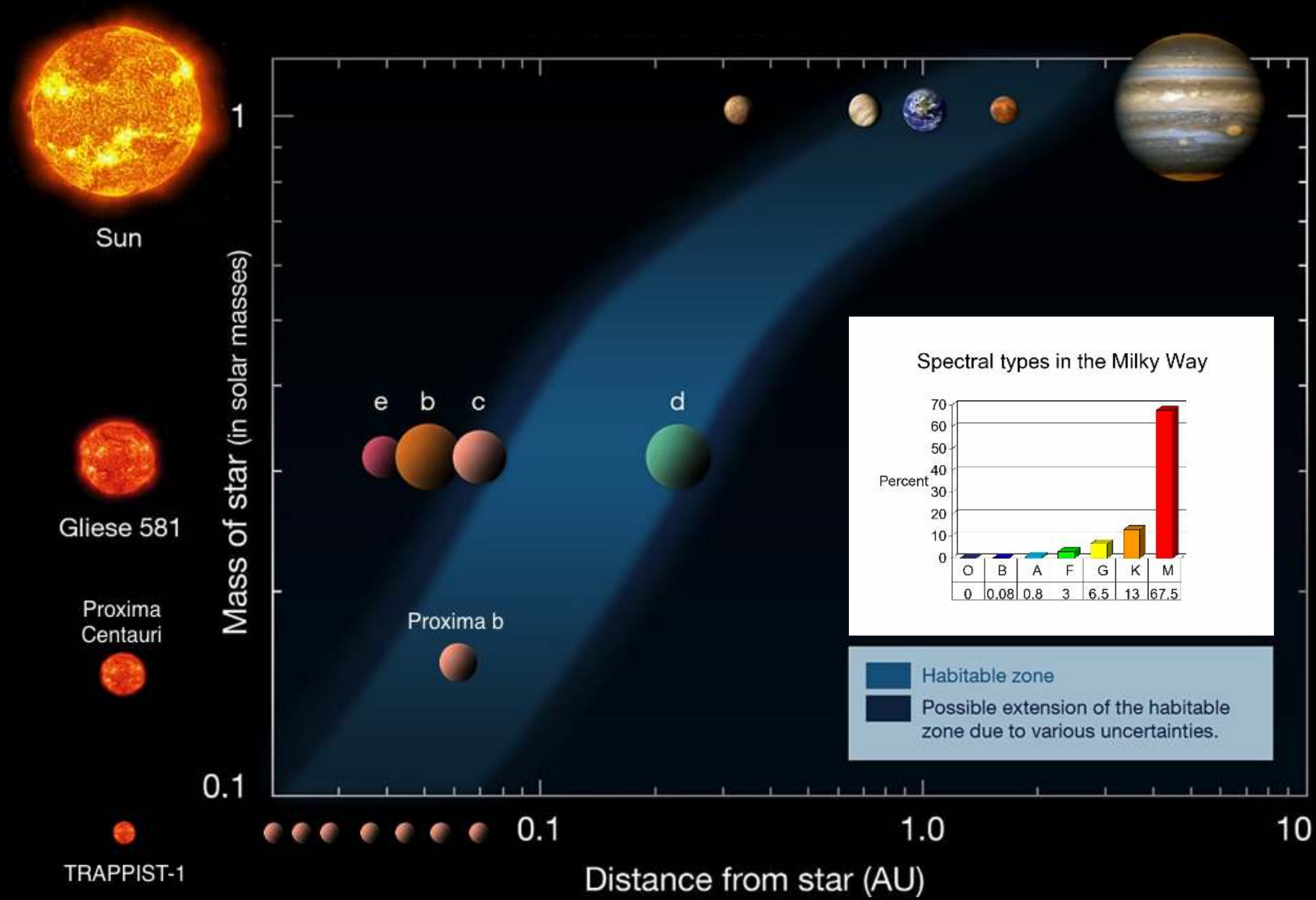

Detecting and Mapping Stellar Magnetic Fields

Magnetic fields and Astrophysics: Zeeman Effect and Spectropolarimetry

1908: First measurement of a magnetic field in an Astrophysical object (Sunspot) by G. E. Hale through the Zeeman Effect.

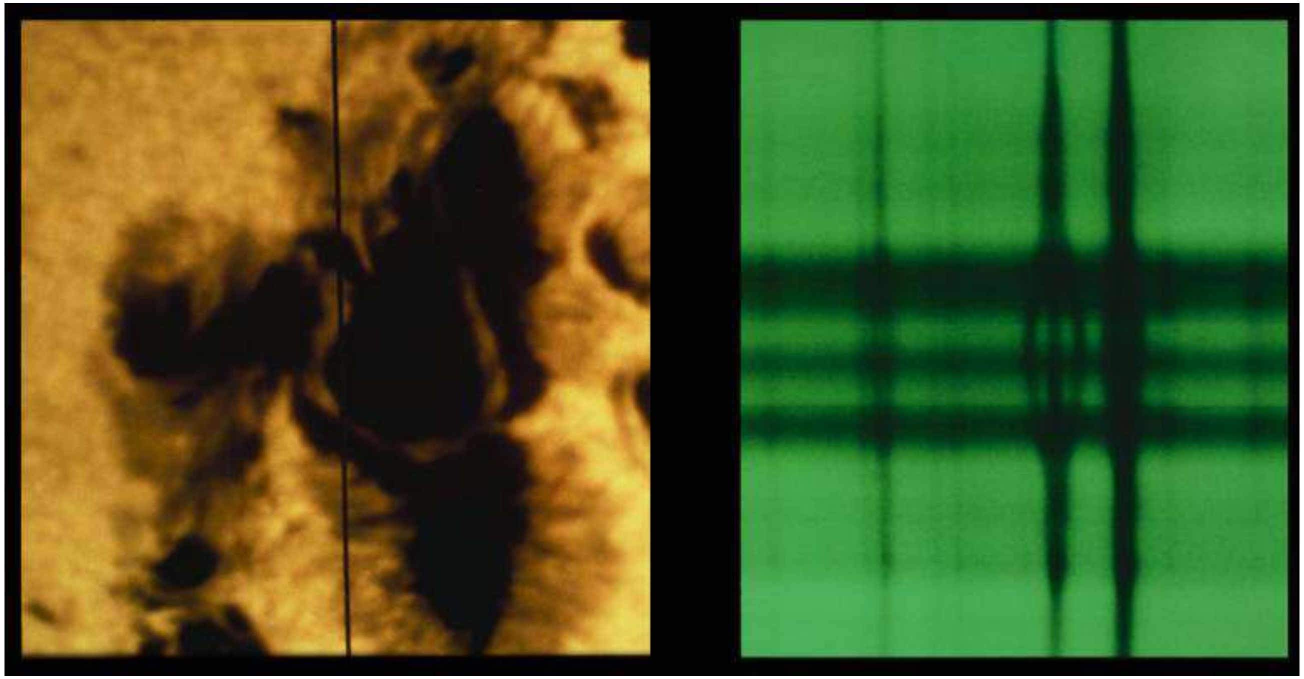

Line Splitting: $\Delta\lambda = 4.67 \times 10^{-13}\, g_{EFF}\, B\, \lambda^2$

Effective Landé Factor: $g_{EFF} = \frac{1}{2}(g_L + g_U) + \frac{1}{4}(g_L + g_U)[J_L(J_L + 1) - J_U(J_U + 1)]$

The Zeeman Effect also induces a signal in the polarization state of the splitting components, depending on the magnetic field geometry and the position of the observer.

(a) Schematic view of Zeeman splitting

(a)

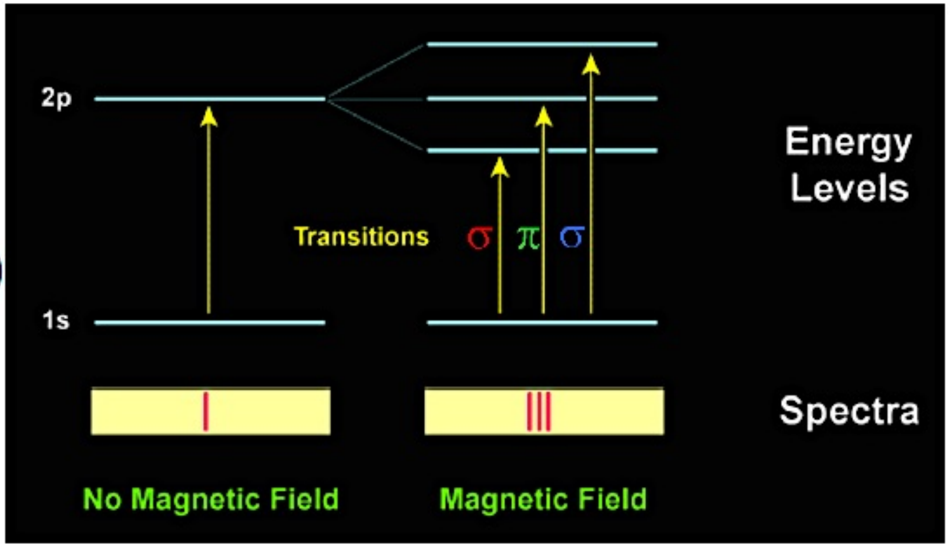

Credit: O. Kochukhov (XXV IAC Winter School)

(b)

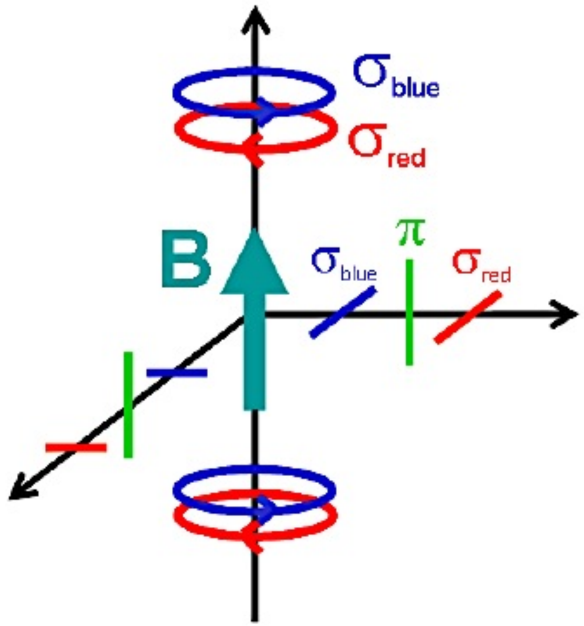

(b) Different polarization states of the Zeeman components

Splitting and Polarization: → Recover the vector properties of **B**.

The polarization state of the light usually is described in the formalism of the Stokes parameters I, Q, U and V.

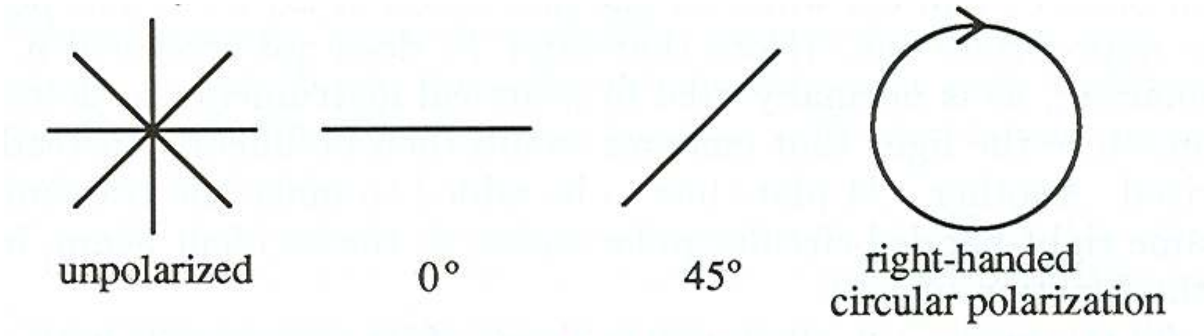

I: Total Intensity.

$I = I_{LIN}(0°) + I_{LIN}(90°) = I_{LIN}(45°) + I_{LIN}(135°) = I_{CIRC}(right) + I_{CIRC}(left)$

$Q = I_{LIN}(0°) – I_{LIN}(90°)$

$U = I_{LIN}(45°) – I_{LIN}(135°)$

$V = I_{CIRC}(right) – I_{CIRC}(left)$

Stokes parameters correspond to + and – of intensities, therefore they can be **measured.**

Spectroscopy: Stokes I
Spectropolarimetry: Stokes I, Q,U and V

Magnetic Field Measurements

The Sun

Helioseismic and Magnetic Imager (HMI): 6173.3 ± 0.1 Å (Fe I line | $g_{EFF} = 2.499$)

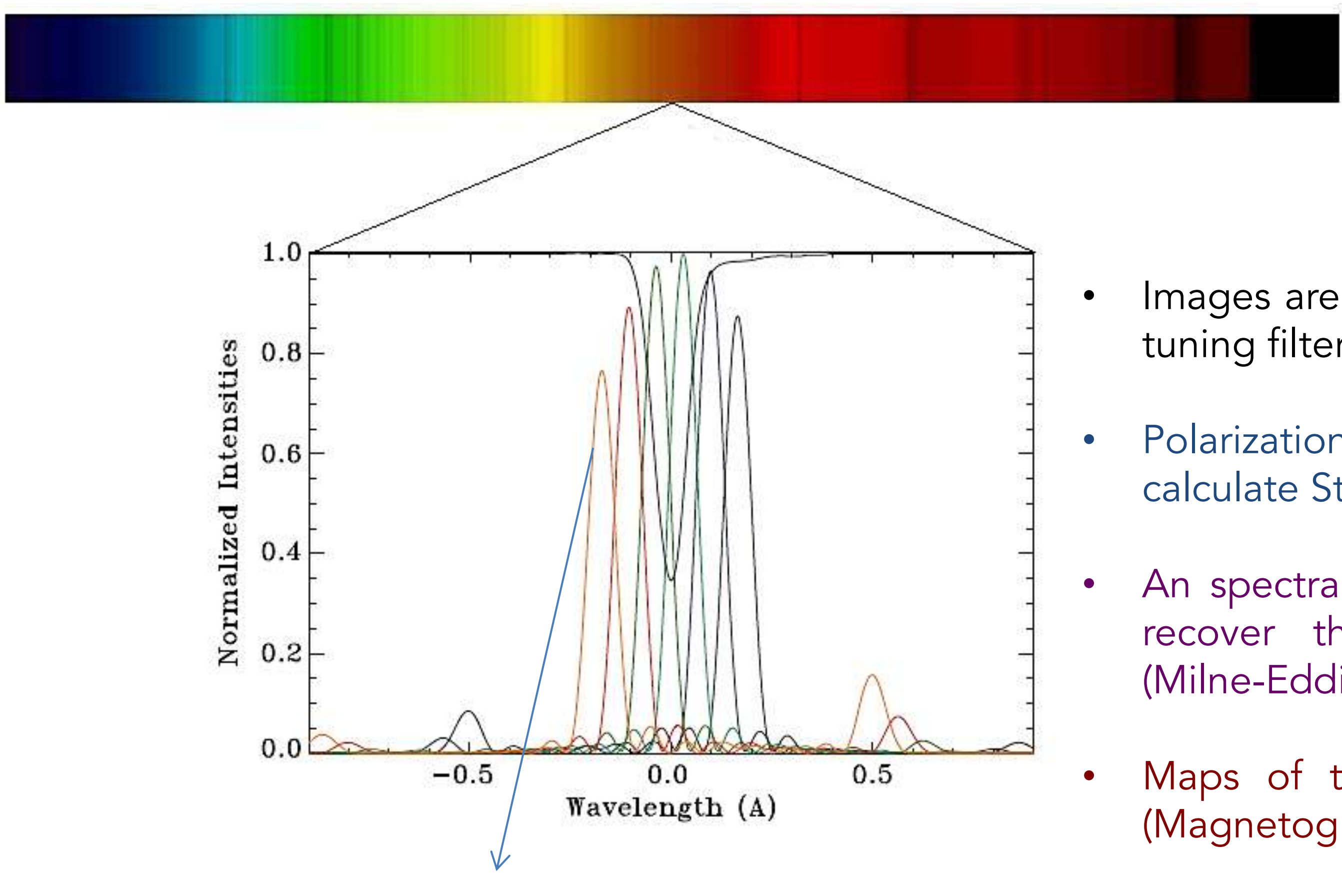

Tuning Filters + Polarization selectors

- Images are generated in each of the 6 tuning filters.
- Polarization selectors are used to calculate Stokes Q, U and V.
- An spectral inversion code is used to recover the vector magnetic field (Milne-Eddington atmosphere).
- Maps of the surface magnetic field (Magnetograms).

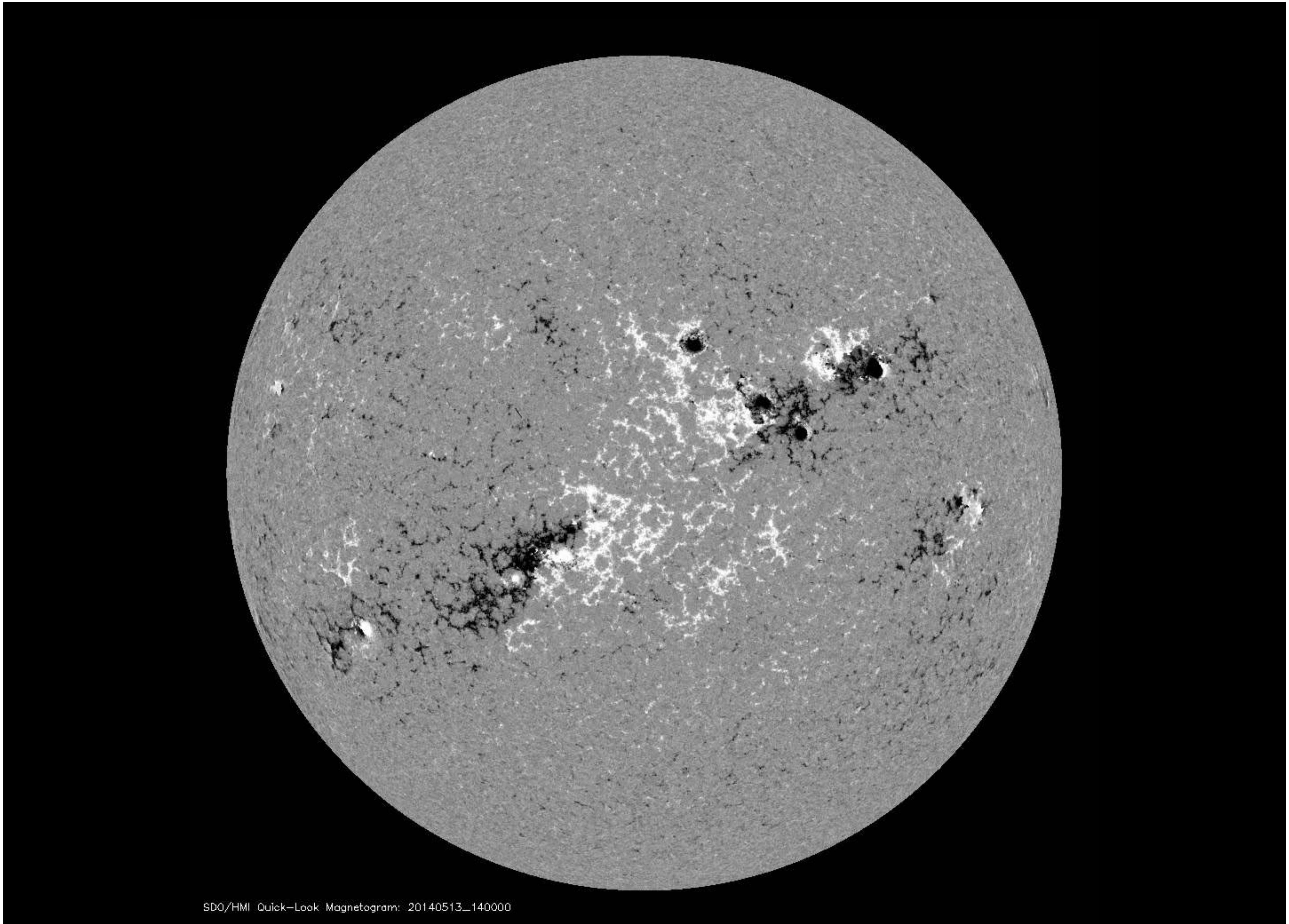
SDO/HMI Quick-Look Magnetogram: 20140513_140000

High resolution spectropolarimetry:

NARVAL@TBL	ESPaDOnS@CFHT	HARPSpol@ESO-3.6m
		
D: 2 m	D: 3.6 m	D: 3.6 m
R ~ 65000	R ~ 70000	R ~ 110000
370 – 1050 nm	370 – 1050 nm	378 – 691 nm

$\Delta\boldsymbol{\lambda} = 4.67 \times 10^{-13}\, g_{EFF}\, B\, \boldsymbol{\lambda}^2$ ⟷ $\Delta v = 1.4\, \boldsymbol{\lambda}_0\, g_{EFF}\, B$

For the typical values of the involved quantities, the Zeeman signature is **below the sensitivity** of current instrumentation.

Solution: Multi – Line Technique

Least Squares Deconvolution (LSD)

(Donati et al. 1997; Kochukhov et al. 2010)

"Add" the polarization signal throughout the entire spectral range.

$$I(v) = 1 - \sum_i w_I^i Z_I(v - v^i), \quad w_I^i = d_i$$

$$V(v) = \sum_i w_V^i Z_V(v - v^i, \boldsymbol{B}), \quad w_V^i = \bar{g}\lambda_i d_i$$

$$Q(v) = \sum_i w_Q^i Z_Q(v - v^i, \boldsymbol{B}), \quad w_Q^i = \bar{G}\lambda_i^2 d_i$$

Sum over all spectral lines (i)

- Self-Similarity
- Scaled by depth, rest wavelengths, and Landé factors

Matrix form:

$$\boldsymbol{V} = \boldsymbol{M} \cdot \boldsymbol{Z}_V$$

Observed spectrum

Line "Mask"

Mean profile

Mean profile for a given line mask and observed spectra:

$$Z_V = \underbrace{(M^{\mathrm{T}} \cdot S^2 \cdot M)^{-1}}_{\text{Inverse Auto-Correlation Matrix}} \cdot \underbrace{M^{\mathrm{T}} \cdot S^2 \cdot V}_{\text{Weighted Cross Correlation}}$$

Inverse Auto-Correlation Matrix

Weighted Cross Correlation

S: Inverse Variance (errors)

(Kochukhov et al. 2010)

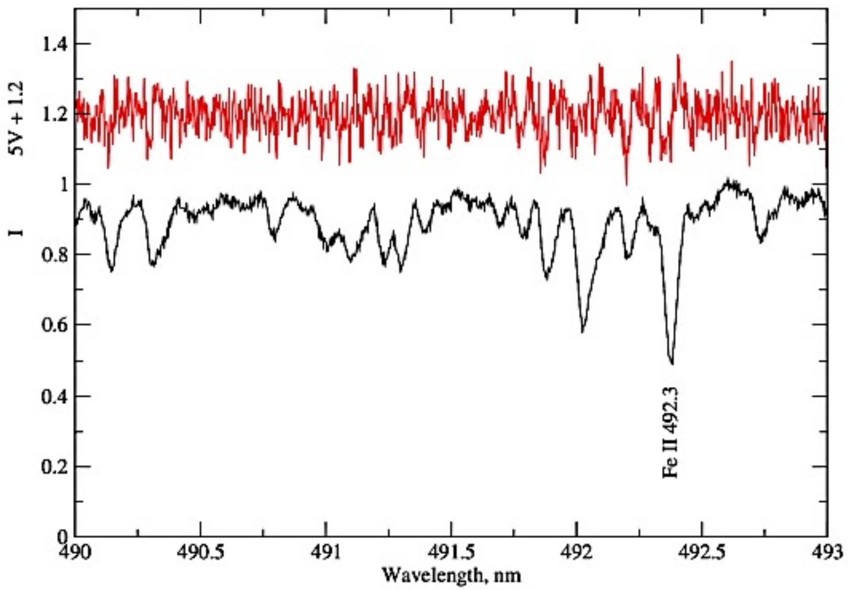

Observed Stokes I and V spectra

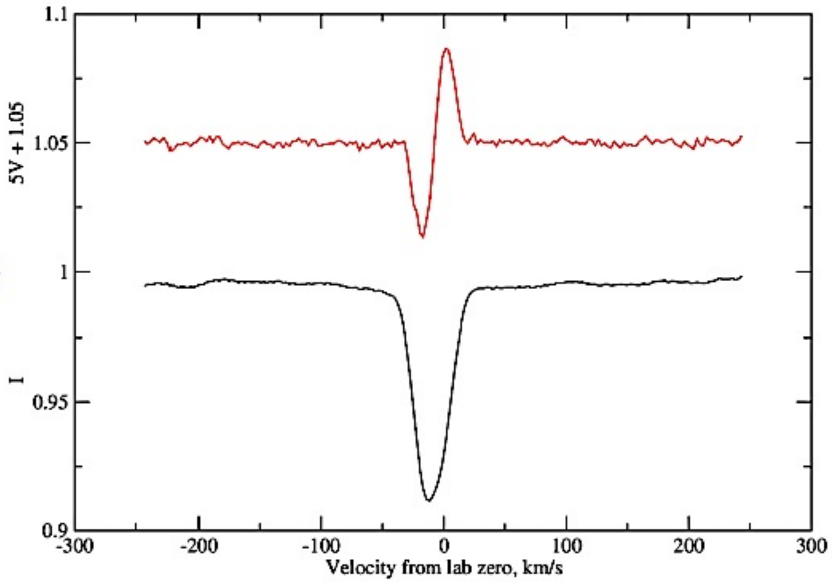

LSD Stokes I and V profiles

S/N Gain ~ √N

N: Number of spectral lines included

Polarimetric Sensitivity: 10^{-5}

Zeeman Doppler Imaging (ZDI): Tomographic inversion technique based on time-series of polarized radiation modulated by rotation.

Usually: Only Stokes V	Requires: Good Phase Coverage
Requires: Stellar Parameters	Assumes: Static Magnetic Field
Ideally: Combined with DI	Includes: Regularization function

Recovers: The large-scale magnetic field distribution on the stellar surface (ZDI maps)

Brightness mapping (DI) **Magnetic field mapping (ZDI)**

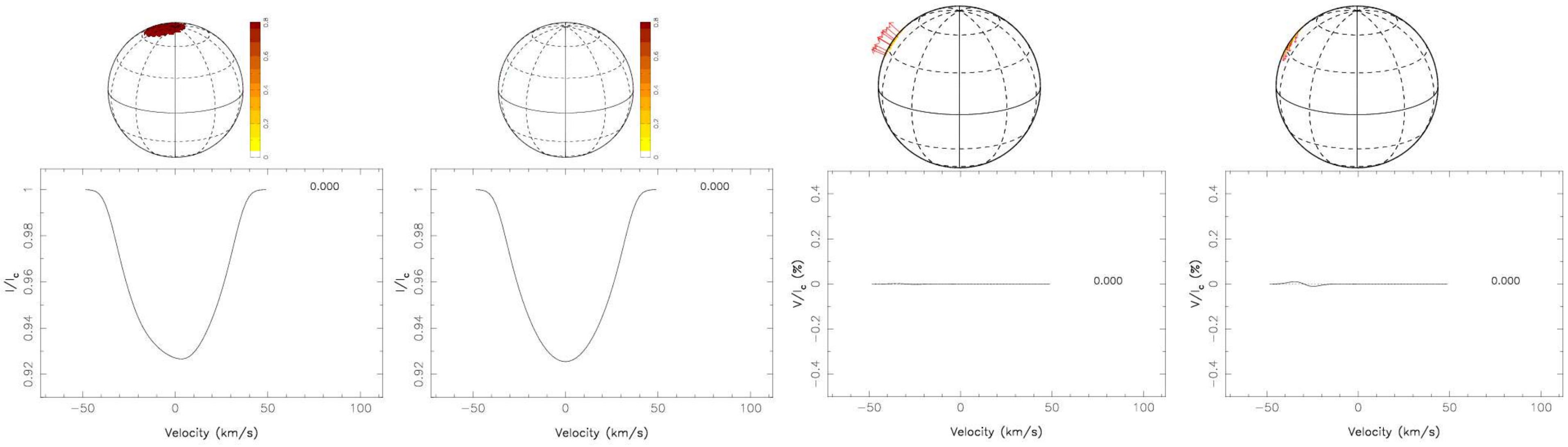

Credit: J.-F. Donati

Some examples:

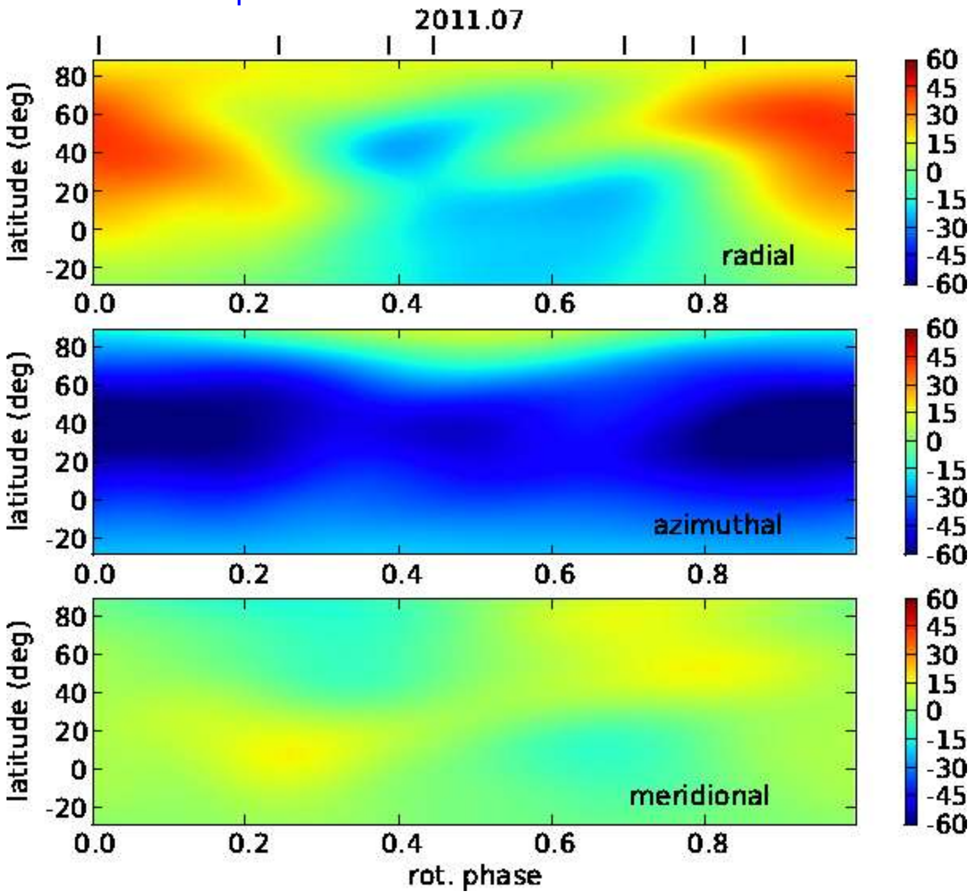

Morgenthaler et al. (2012)

ξ Boo A (G8V)

M = 0.85 $M_{\odot}$

P_{ROT} = 6.43 days

T_{EFF} = 5600 K

vsin(i) = 3.0 km/s

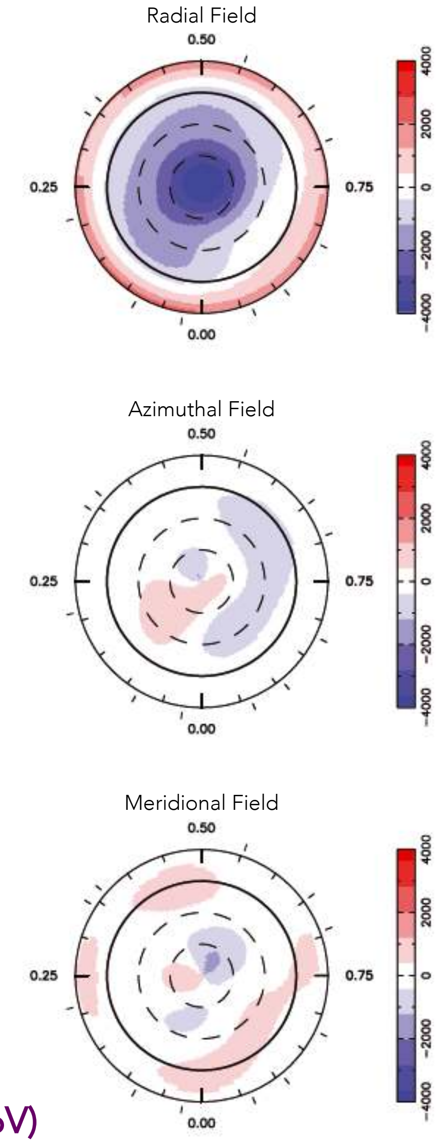

Morin et al. (2010)

WX UMa (M6V)

M = 0.1 $M_{\odot}$

P_{ROT} = 0.78 days

T_{EFF} ≈ 2800 K

vsin(i) = 5.0 km/s

HD 1237 (G8V, ~880 Myr)

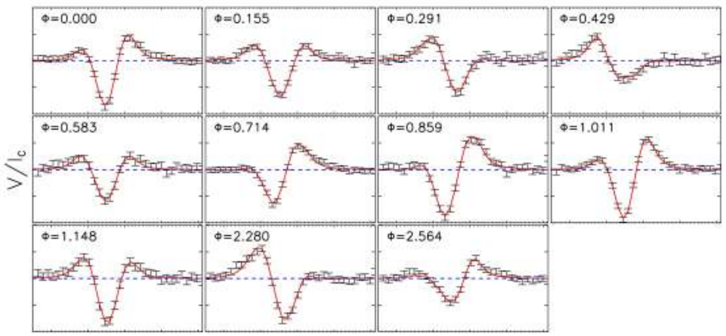

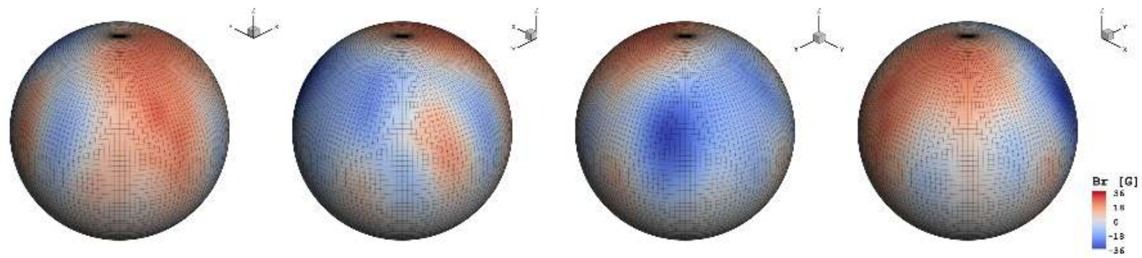

Alvarado-Gómez et al. (2015)

ε Eridani (K2V, ~440 Myr)

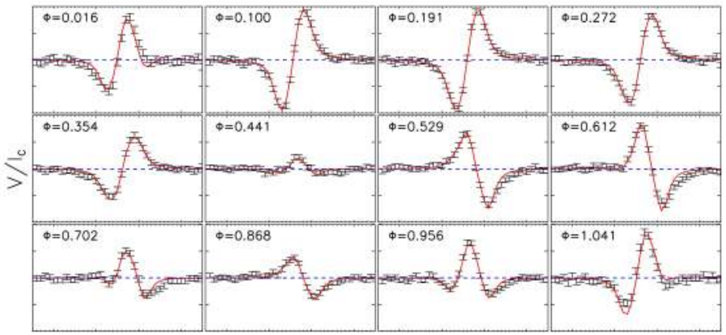

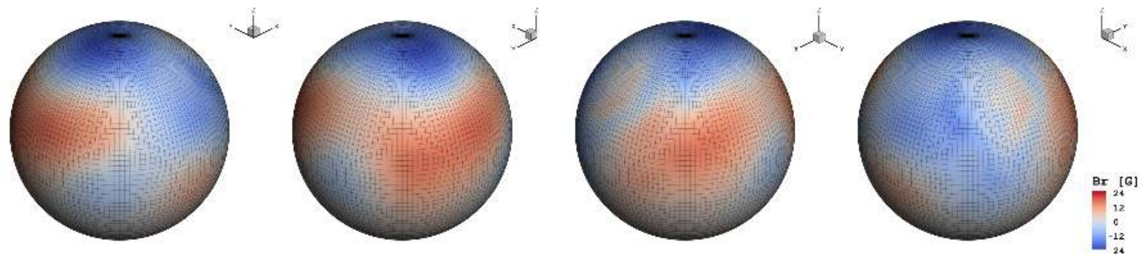

Piskunov et al. (2011); Jeffers et al. (2014); Alvarado-Gómez et al. (2016a)

HD 147513 (G5V, ~450 Myr)

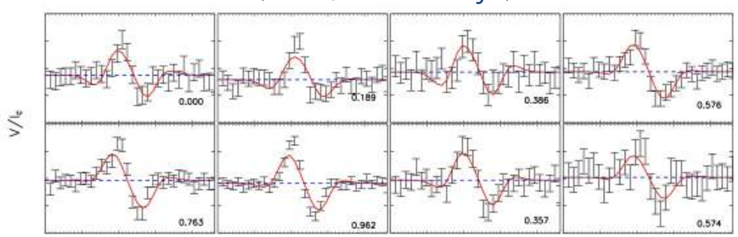

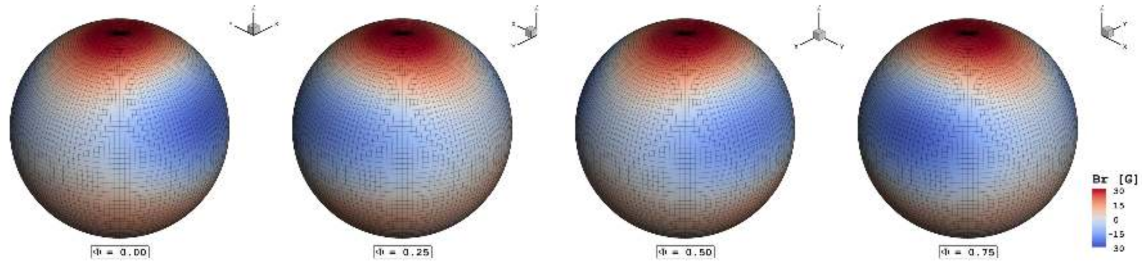

Hussain, Alvarado-Gómez et al. (2016)

Magnetism in cool main sequence stars

Donati & Landstreet (2009); Donati (2011); Kochukhov (2021)

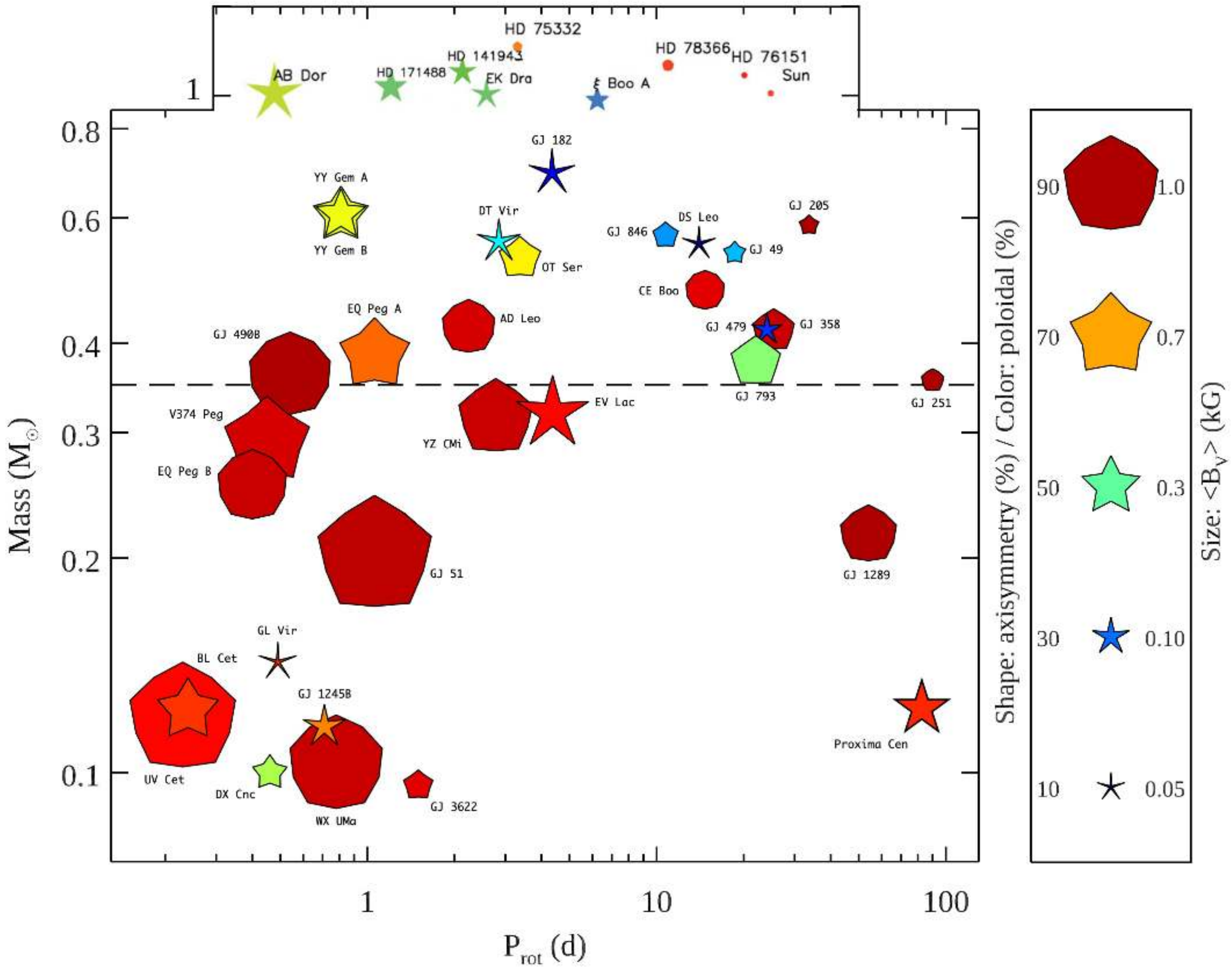

Sizes: Field Strength
(3 – 1000 G)

Color: Main Geometry
(Red: Poloidal | Blue: Toroidal)

Shapes: Symmetry
(Decagons: Axisymmetric
Stars: Non-Axisymmetric)

Instrumentation in High-Resolution Spectropolarimetry

D = 2 m | R ~ 65000
λ ~ 370 – 1050 nm

D = 3.6 m | R ~ 70000
λ ~ 370 – 1050 nm

D = 3.6 m | R ~ 120000
λ ~ 378 – 691 nm

New instruments/upgrades:

NEO NARVAL

RV precision < 3 m/s
Now observing!

SPIRou

R ~ 75000 | **λ** ~ 0.98 – 2.35 μm
RV precision ~ 1 m/s
Now observing!

CRIRES+

R ~ 50k / 100k | **λ** ~ 1.0 – 2.7 μm
RV precision ~ 1–2 m/s
[8m-class telescope]
First Light: ~ 2021

PEPSI

R ~ 120k | **λ** ~ 384 – 913 nm
RV precision ~ 1–2 m/s
[8m-class telescope]
Now observing!

Studying the Space Weather in Cool Main-Sequence Stars

The Space Weather Modeling Framework (SWMF)

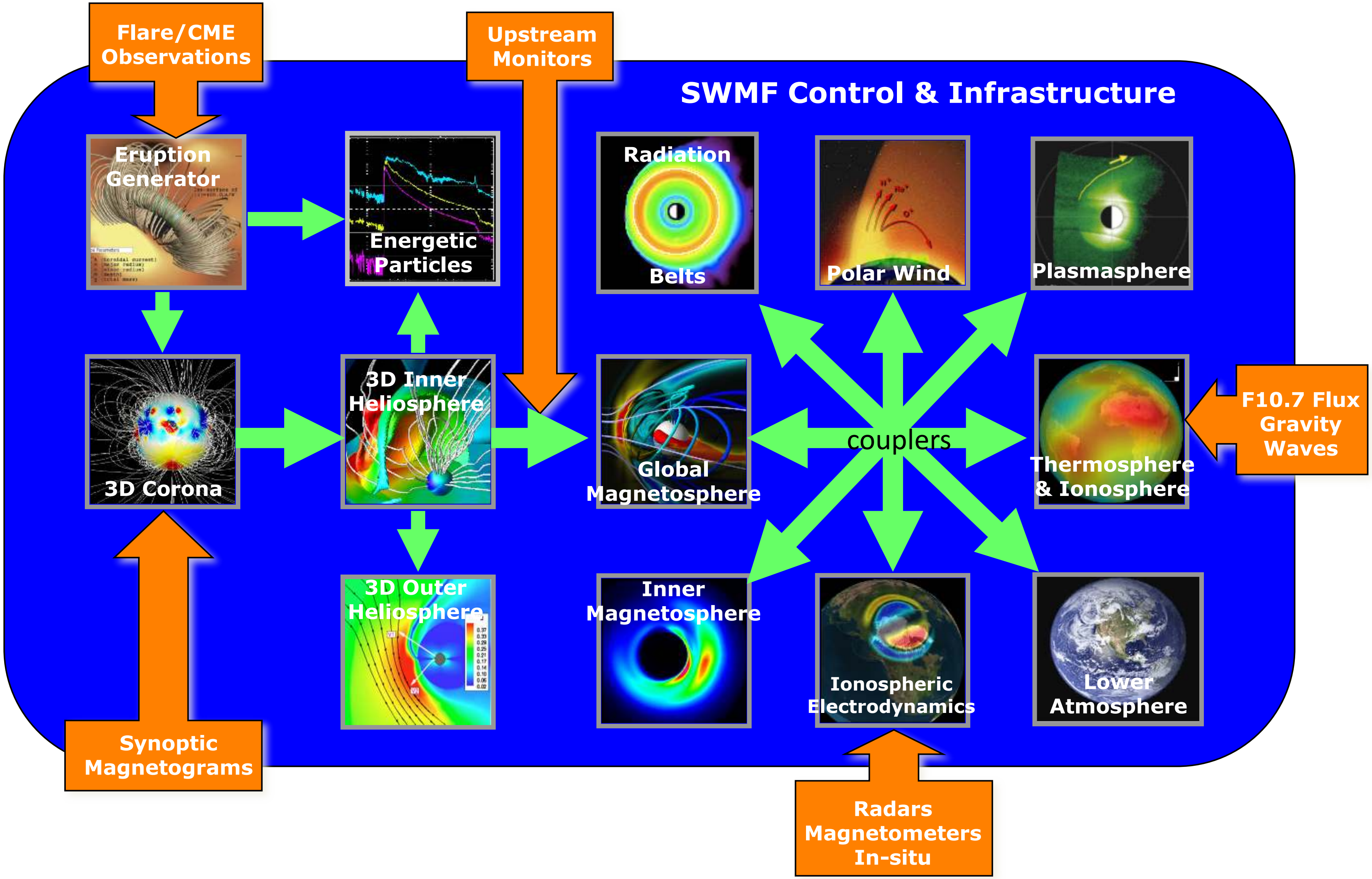

Toth+ (2012), Gombosi+ (2018)

3D Coronal Structure

Coronal features: Field topology

Coronal thermodynamic conditions: Field strength (Unsigned flux)

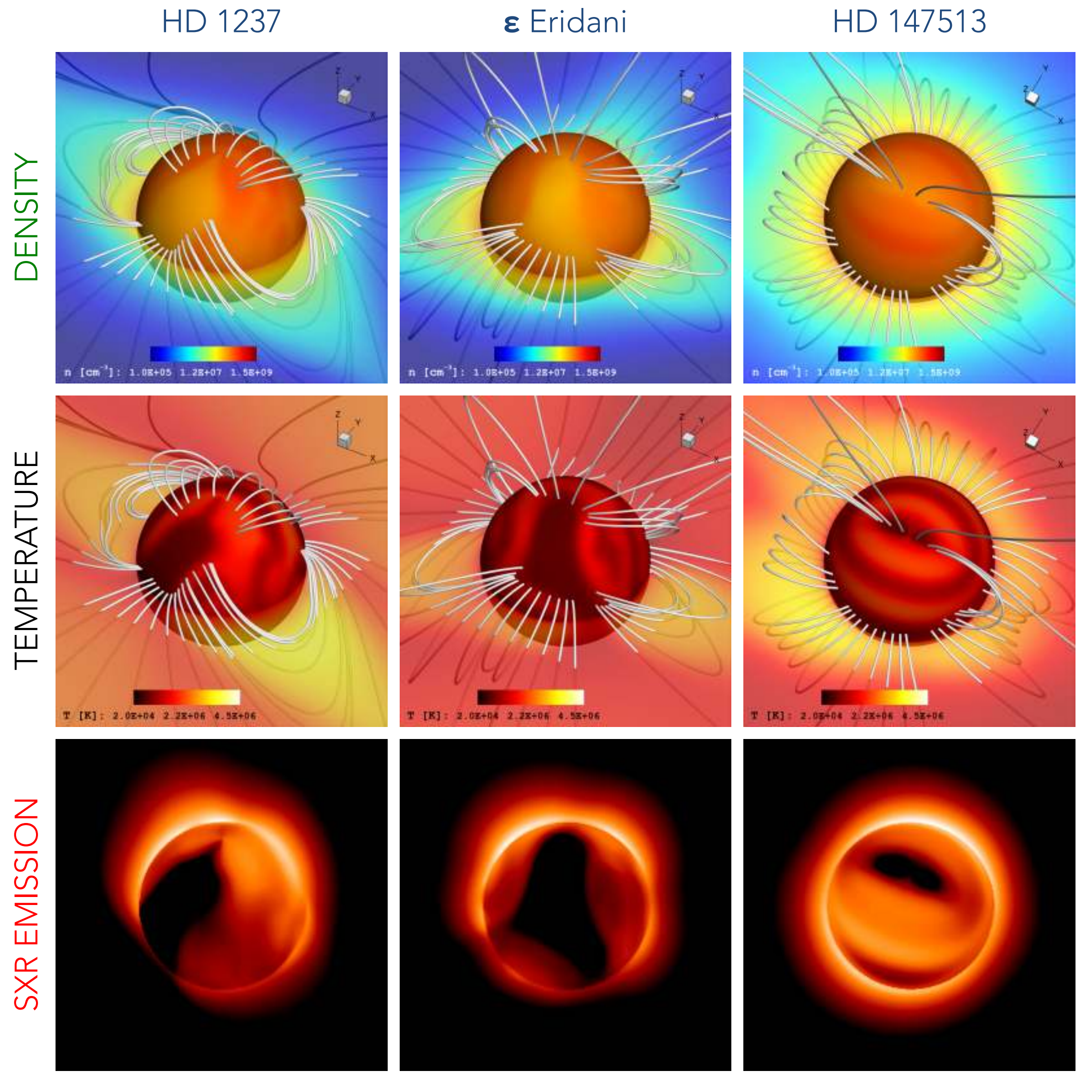

Emission Measure (EM) Distribution

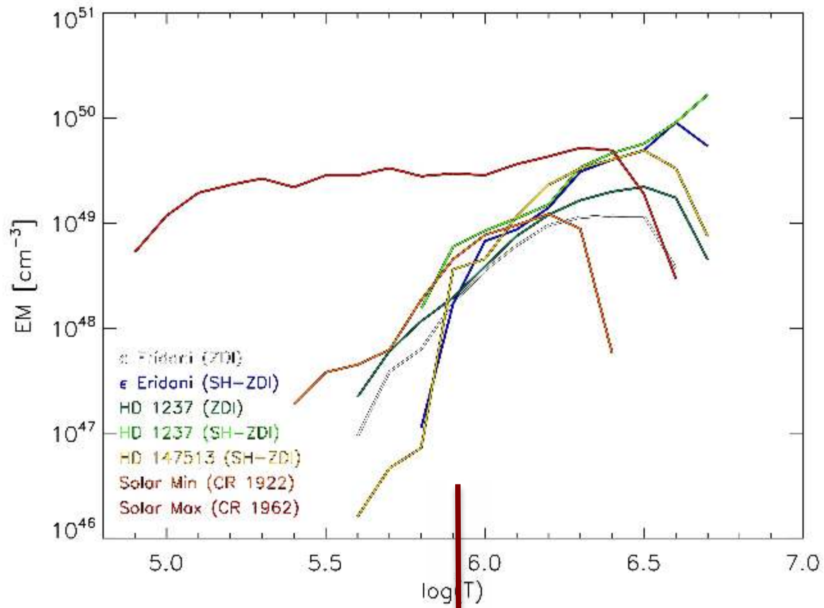

Synthetic Spectra

Alvarado-Gómez et al. (2016a)

Solar Wind Structure

Solar Minimum | Solar Maximum

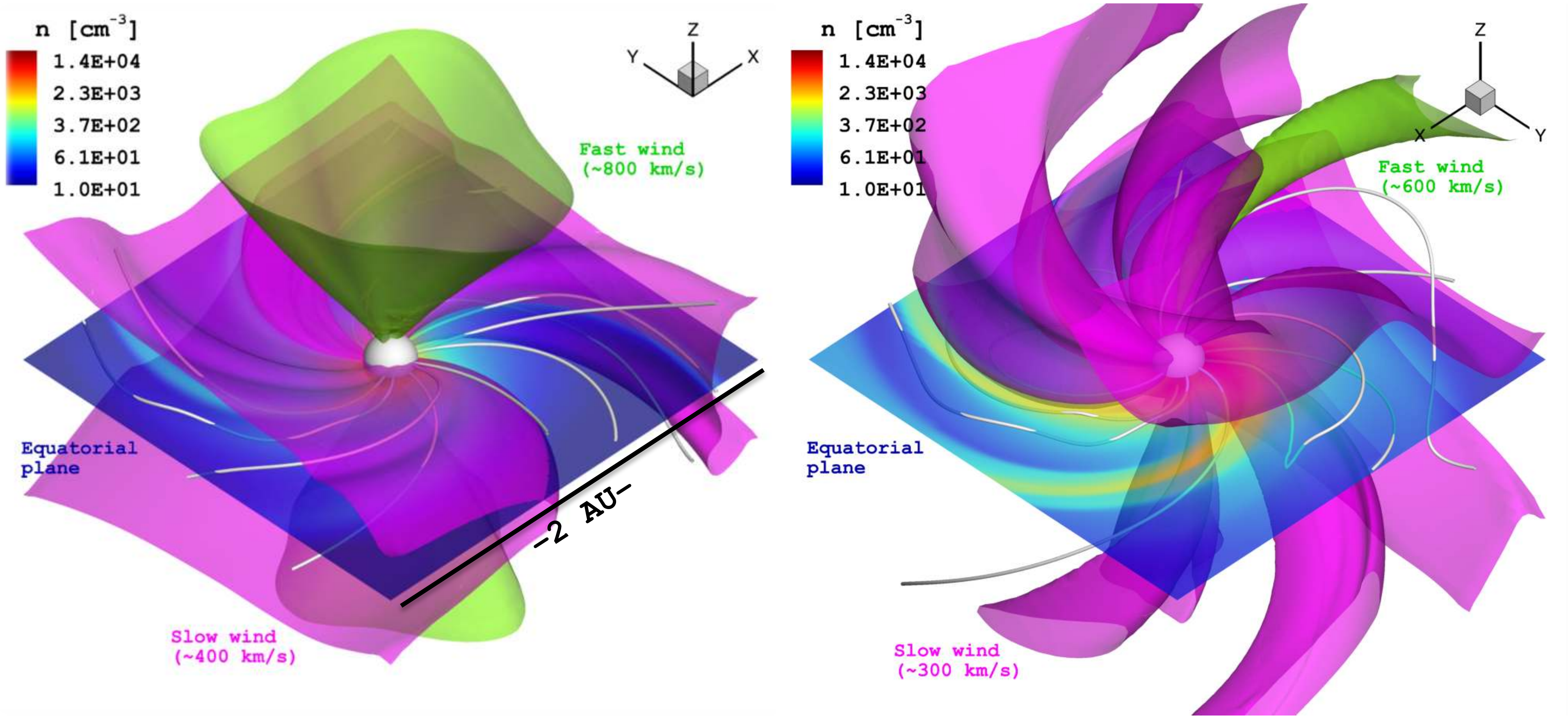

Alvarado-Gómez et al. (2016b)

Fast-wind from the poles
(Coronal Holes)

Slow-wind along the Equatorial plane
("Ballerina Skirt")

Slow-wind dominates the structure
(closed-field regions)

Almost no fast wind regions
Increased complexity

HD 1237 (G8V, ~880 Myr)

Alvarado-Gómez et al. (2016b)

Jupiter–mass planet
located at ~ 0.5 AU
(P_{ORB} = 133.7 ± 0.2 days, e = 0.49)
(Naef et al. 2001)

Strong wind-planet interactions along the orbit

Potentially detectable in Radio
(F_R ~ 12 mJy)

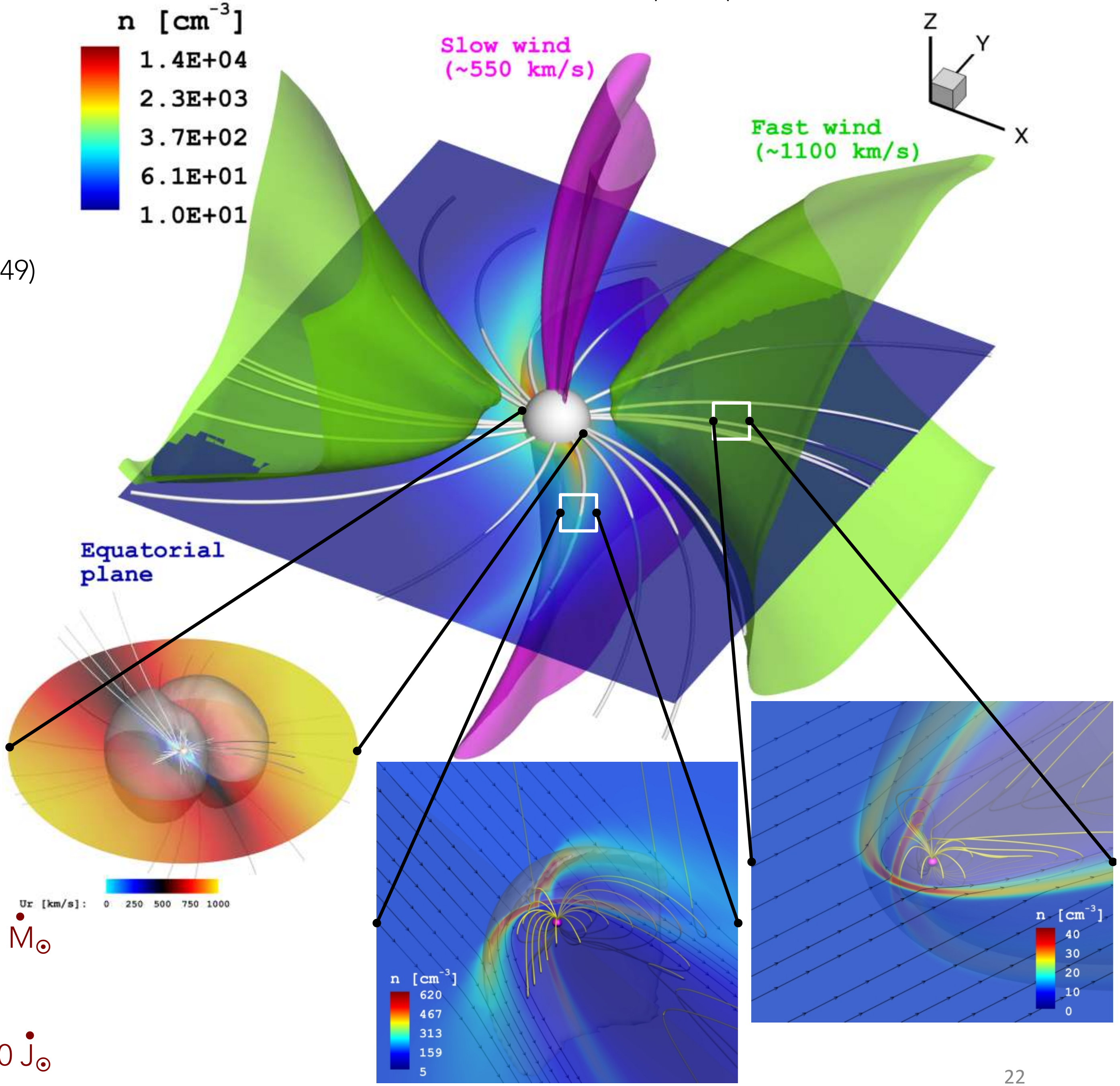

Mass loss: ~3 – 7 $\dot{M}_\odot$

Angular momentum loss: ~7 – 60 $\dot{J}_\odot$

Space Weather of the TRAPPIST-1 System

(Garraffo et al. 2017)

TRAPPIST-1 (M8V)
$M_{\star} \simeq 0.08\ M_{\odot}$
$R_{\star} \simeq 0.114\ R_{\odot}$
$P_{ROT} \simeq 1.4$ days

7 planets within 0.01 – 0.063 AU
($P_{ORB} \simeq 1.5 – 20$ days)

(Guillon et al. 2017, 2016; Luger et al. 2017)

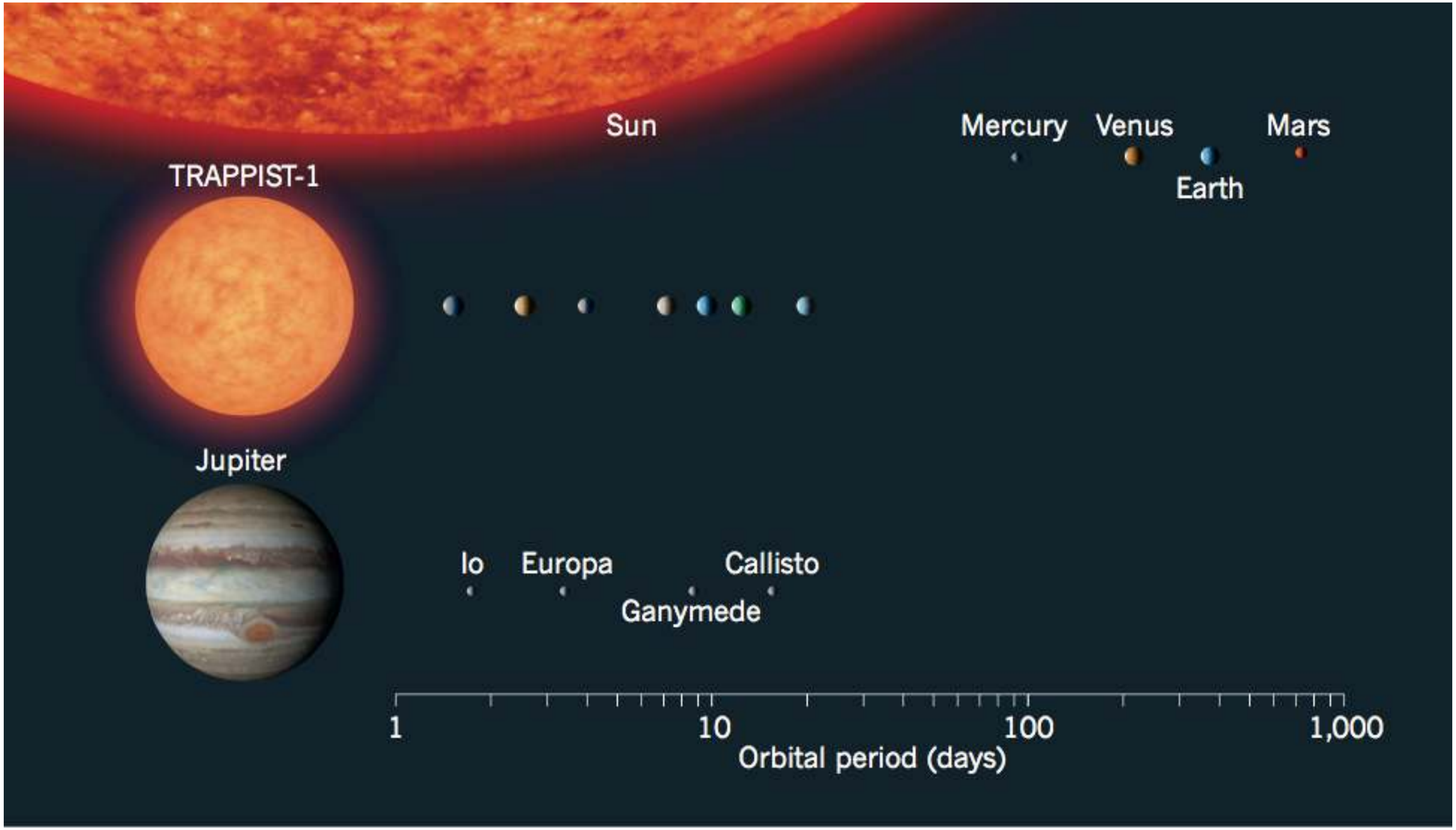

Space Weather of the TRAPPIST-1 System

(Garraffo et al. 2017)

TRAPPIST-1 (M8V)
$M_\star \simeq 0.08\ M_\odot$
$R_\star \simeq 0.114\ R_\odot$
$P_{ROT} \simeq 1.4$ days

7 planets within 0.01 – 0.063 AU
($P_{ORB} \simeq 1.5 – 20$ days)

(Guillon et al. 2017, 2016; Luger et al. 2017)

No ZDI map available ➛ Proxy: GJ3220
(M6.5V, $P_{ROT} \simeq 1.5$ days; Morin et al. 2010)

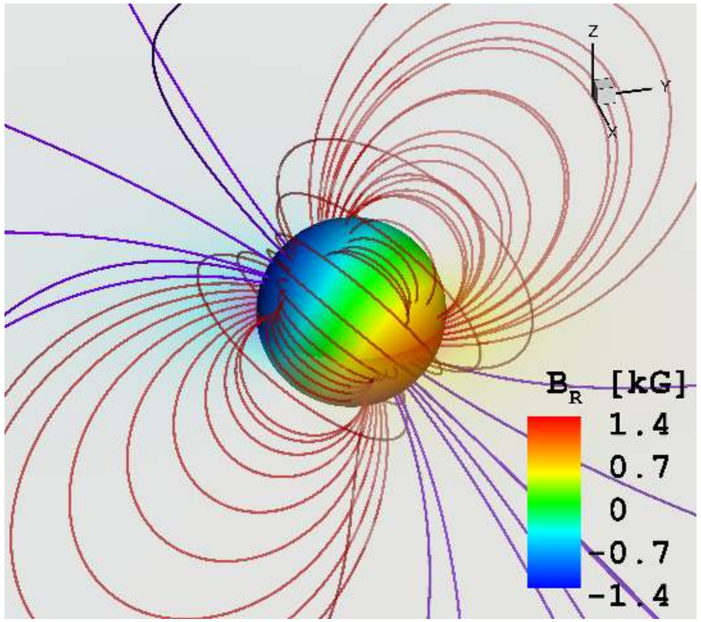

- Extreme environment for all planets: n and Ur
- Depending on $B_\star$: 4/6 planets would be located inside the Alfvén Surface (cf. Cohen et al. 2014).

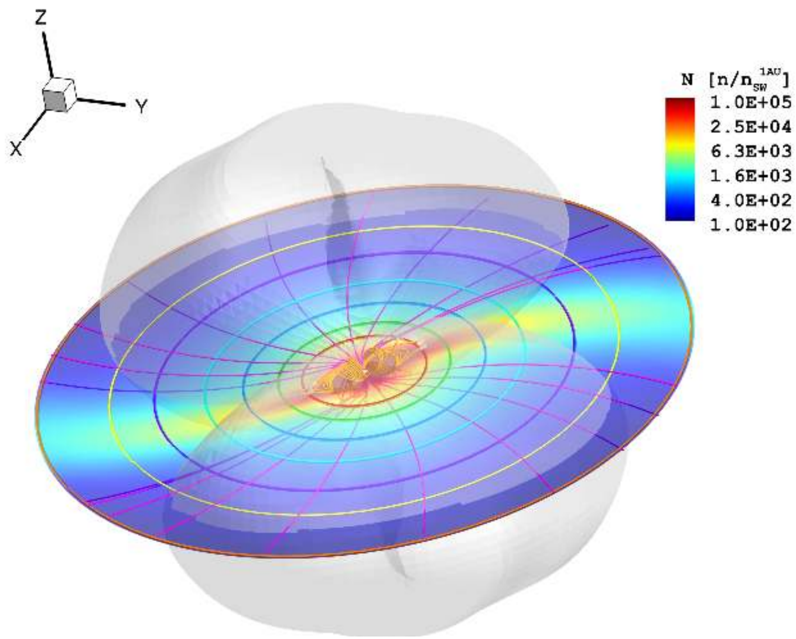

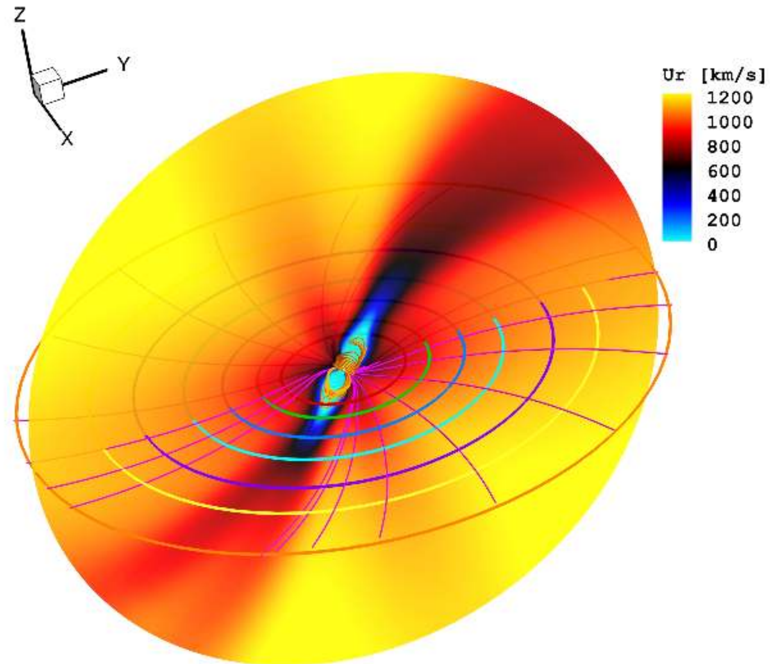

Wind Environment of Barnard's Star b

Barnard's Star (M3V)
$M_\star \simeq 0.144\ M_\odot$
$R_\star \simeq 0.196\ R_\odot$
$P_{ROT} \simeq 130$ days

Super-Earth orbiting around 0.4 AU
($P_{ORB} \simeq 232.8$ days)
(Ribas et al. 2018)

No ZDI map available ➛ 3 Different proxies
(Based on Spectral Type and Rossby Number)

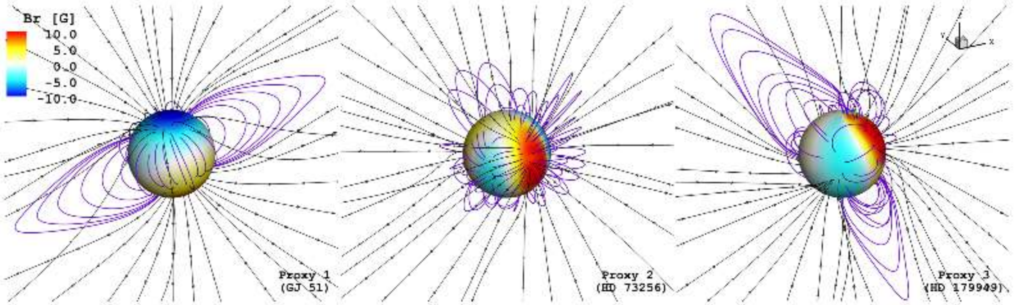

Wind dynamic pressure: Comparable to present-day Earth values.

Similar results for all proxies.

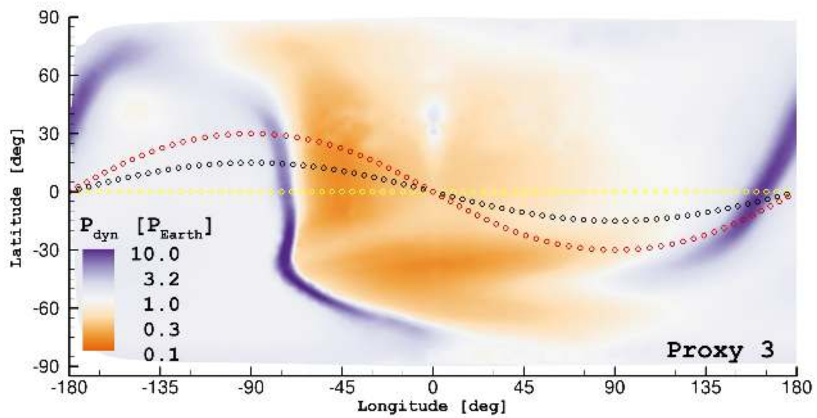

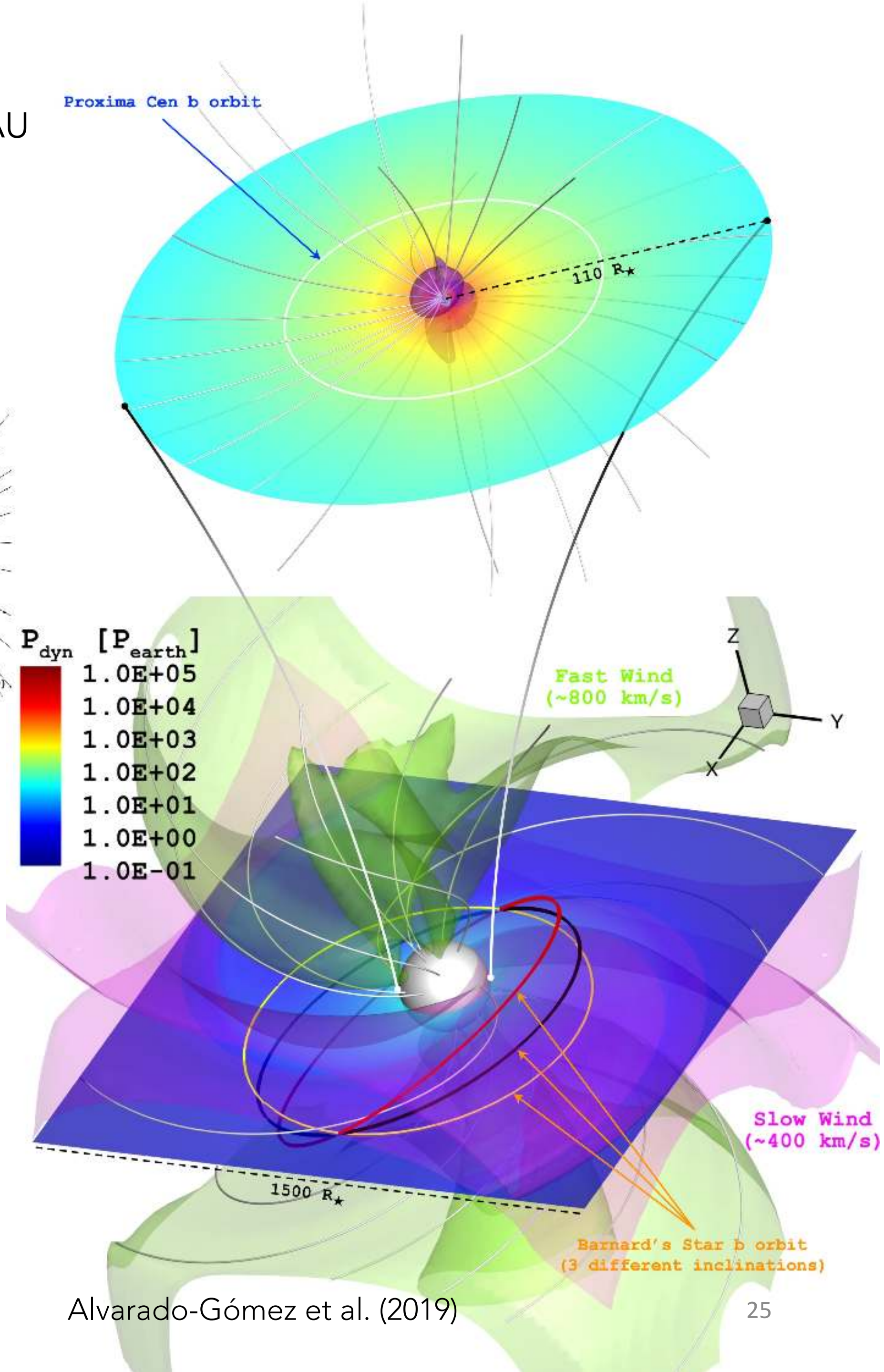

Alvarado-Gómez et al. (2019)

Application: Studying Coronal Mass Ejections (CMEs) in Active Stars

Solar Flares – CMEs: generalities and association

- Flares: Sudden energy release in the corona involving particle acceleration, radiation, and plasma heating.
- CMEs: "Localized" release of plasma and magnetic field into the solar/stellar wind (plasmoids/filament eruptions).
- Solar statistics: Large flares are nearly always accompanied by a CME (Yashiro & Gopalswamy 2009).

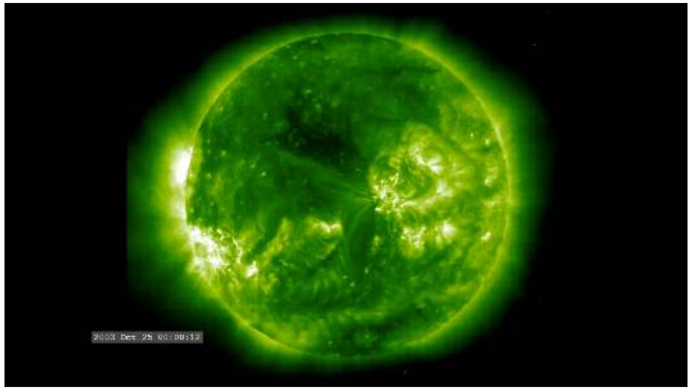

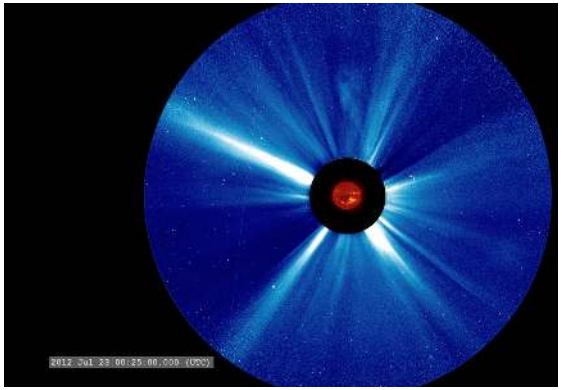

Extension to more active stars?

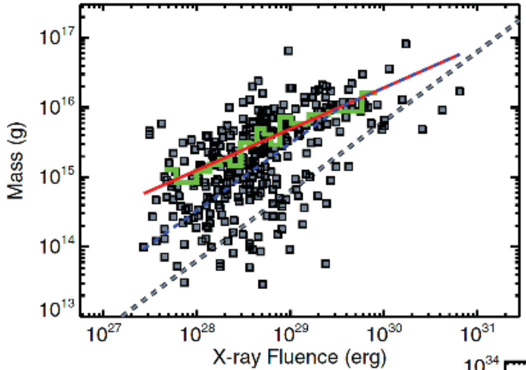

Study of Drake+ 2013:
(see also Odert+ 2017)

Consequences of extrapolating the observed mass and kinetic energy of CMEs associated with solar flares to more active stars.

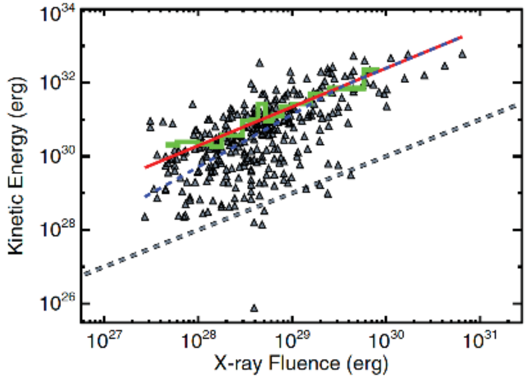

A saturated Sun-like star (L_X ~ 10^{30} erg/s) would have:

CME-Mass loss rate: $\dot{M} \sim 5 \times 10^{-10} \, M_\odot \;\; \mathrm{yr}^{-1}$

CME-Kinetic energy requirement: $\dot{E}_{ke} \sim 0.1 \, L_\odot$

Conclusion: The flare-CME relations (mass/energy) must flatten out for large energies (≥ 10^{31} ergs)

Possible solution: Suppression of CMEs by an overlying magnetic field

Stellar observations

Donati & Landstreet (2009), Donati (2011); Kochukhov (2021)

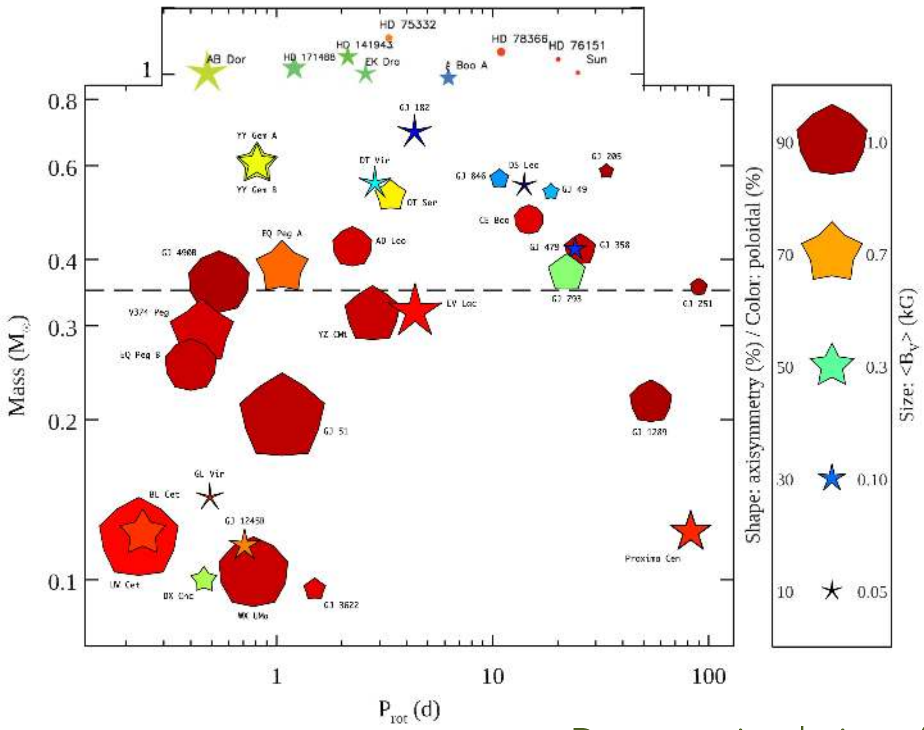

Solar observations

Lin+ (2016)

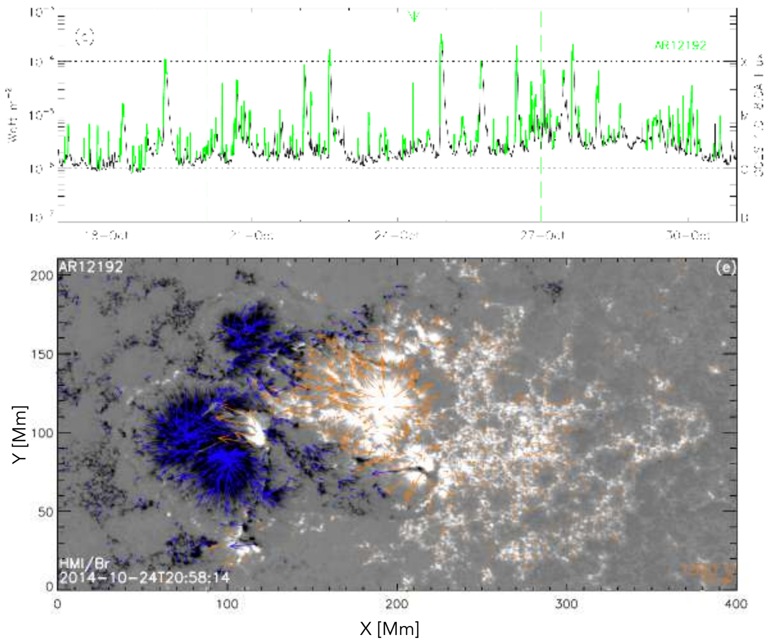

Dynamo simulations (Fully-convective stars)

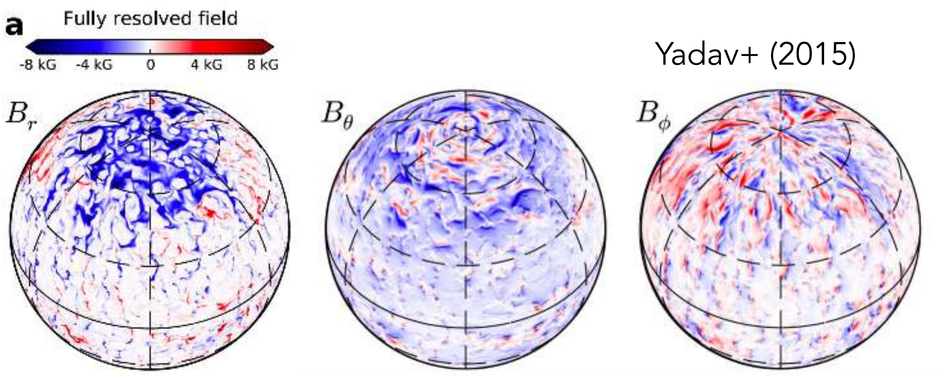

Yadav+ (2015)

3D CME simulations: Flux rope eruption models

Eruption of a twisted flux rope starting from the steady-state corona/wind solution (AWSoM; van der Holst+ 2014)

Validated against Solar CME observations (Jin+ 2017)

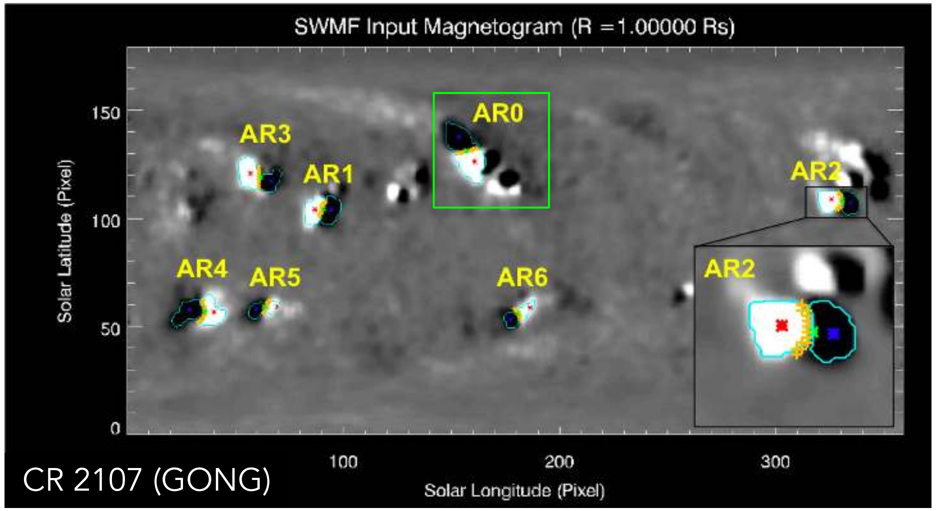

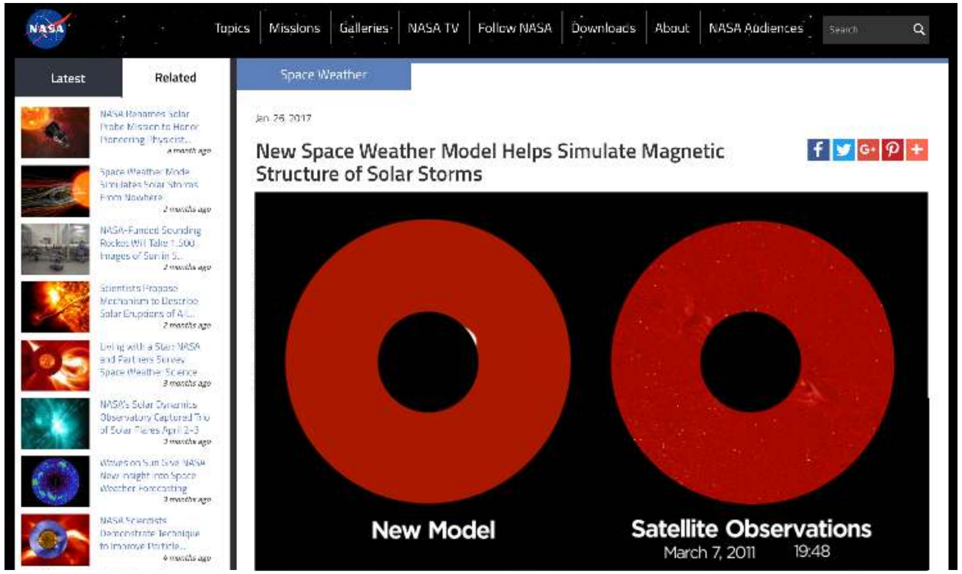

Jin+ (2017)

Parameters from the calibration study of the CME model applied on a "younger Sun".

Simulation domain: 1 – 50 $R_\odot$

Grid: Spherical + High-res spherical wedge (25 $R_\odot$).

1 hour wall-clock time for each CME simulation.

CR 2107 + 75 G Dipole

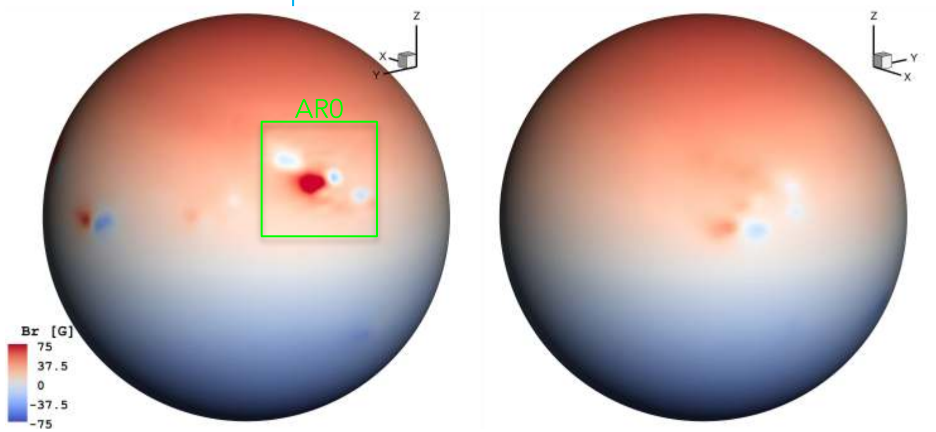

Alvarado-Gómez+ (2018)

Results:

Confined CMEs

Alvarado-Gómez+ (2018)

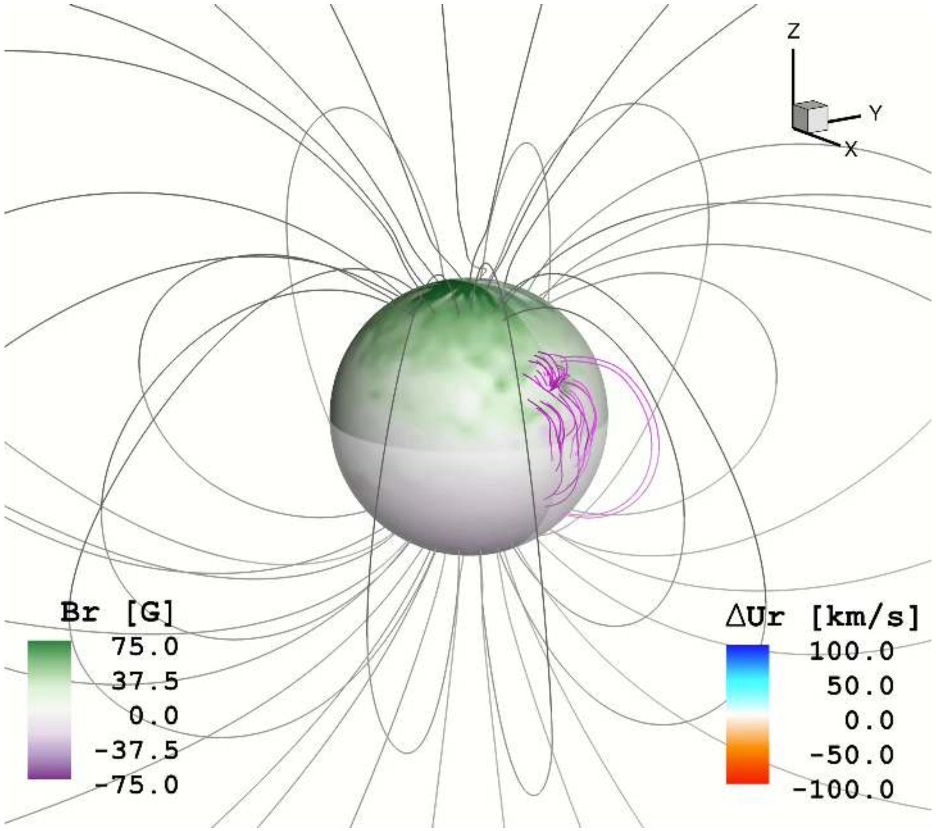

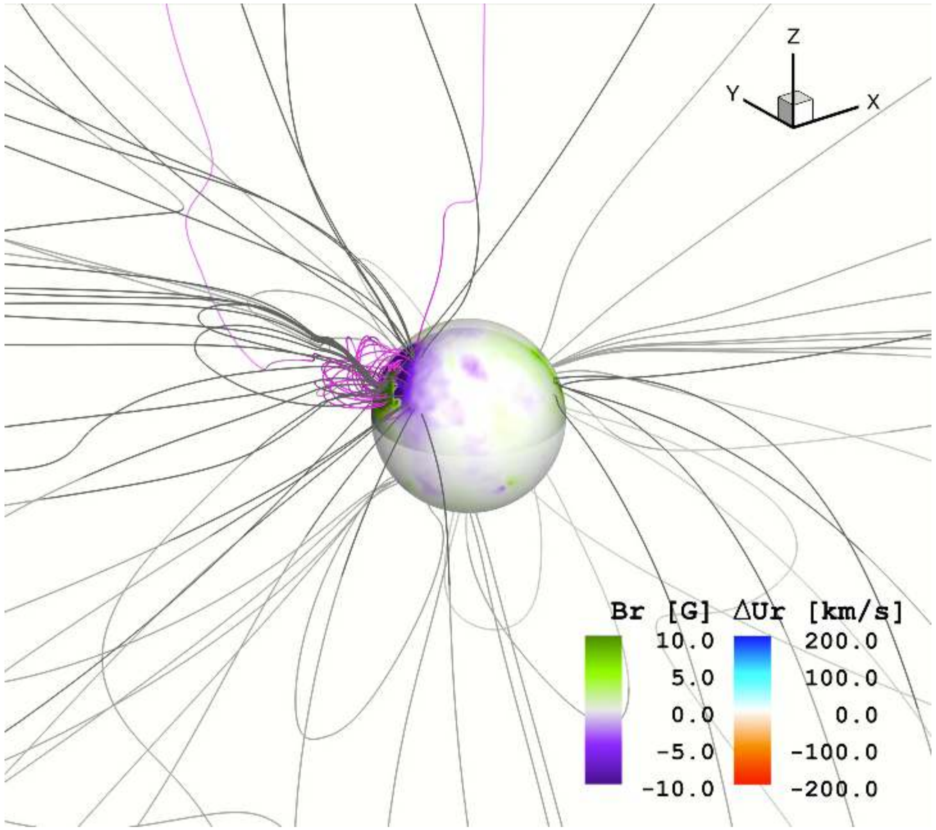

Φ_P = 1.94 x 10^{22} Mx
(Equivalent GOES Class Flare: X5.0)

Solar CME simulation

The coronal material rises following the overlying field lines.

The perturbed plasma remains confined within the region of the lower corona.

Solar simulations: ~2500 – 3000 km/s
(CME-Speed – Φ_P Relation; Jin+ 2017)

Results: CME radial speed and mass

Alvarado-Gómez+ (2018)

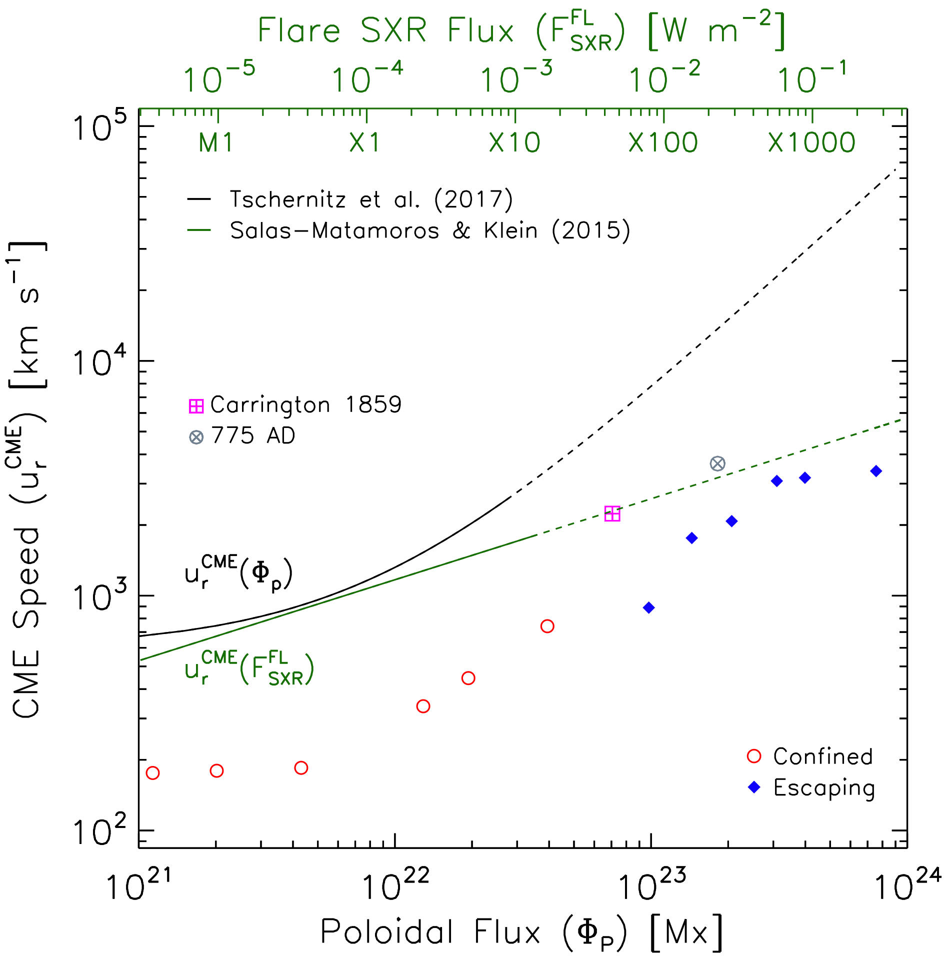

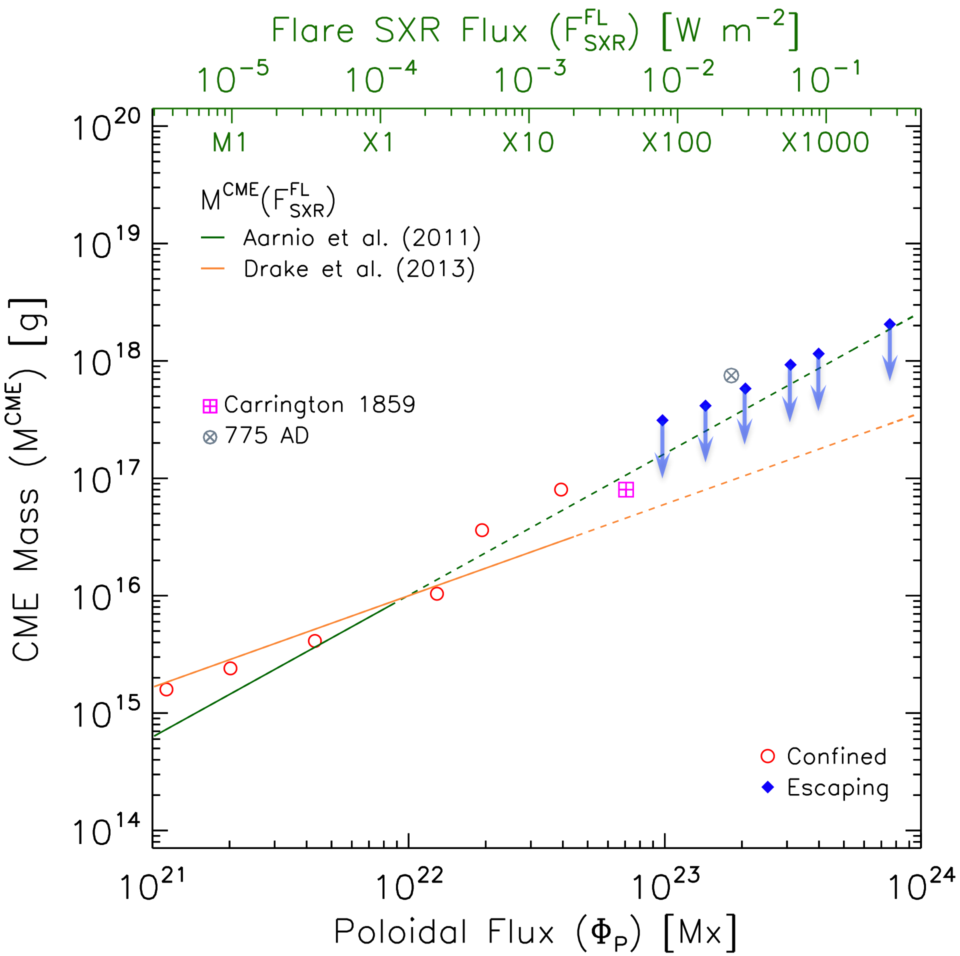

The large-scale field slows down all the CMEs.

The radial speed reduction is larger for confined events than for the escaping ones.

The perturbed coronal mass behaves similarly between confined and escaping events.

Simulated "CME masses" are consistent with extrapolations from Solar data.

Results: CME Suppression threshold

Alvarado-Gómez+ (2018)

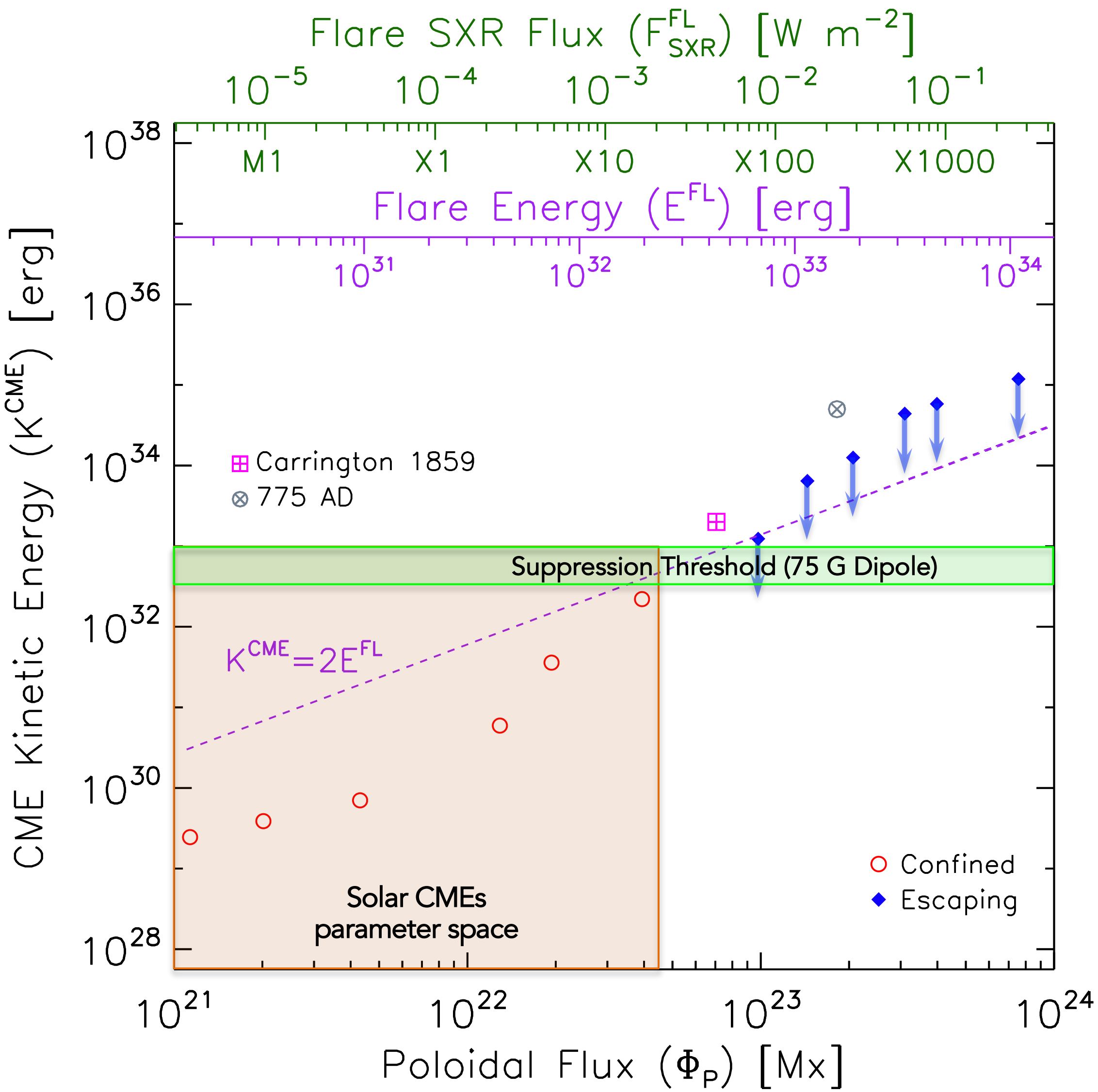

Escaping CMEs are **less energetic** than expected.

Historical candidates and a recent direct detection of a stellar CME show this!

Magnetic suppression would mitigate small/moderate CMEs in active stars.

Only "monster" CMEs would be able to escape (c.f. Moschou+ 2017).

Until very recently, there were no definitive detections of stellar CMEs
(e.g., Leitzinger+ 2014, Crosley+ 2016, Villadsen 2017)

Moschou+ (2019): A comprehensive compilation of historical stellar CME candidates.
(see also Vida+ 2019)

CME Mass | CME Kinetic Energy

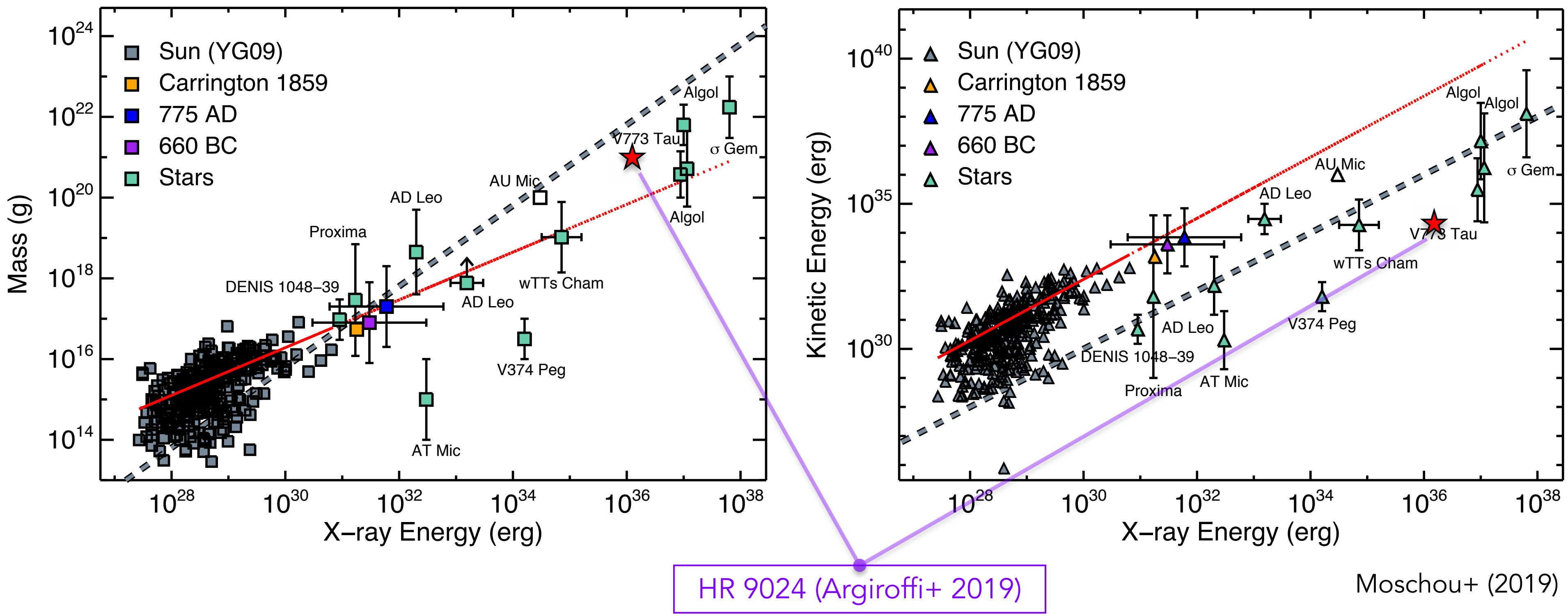

Moschou+ (2019)

Red line: Fit to the solar data (and extrapolation)

Dashed line: Constant ratio of CME mass loss to flare X-ray energy loss.

Parity between flare X-ray and CME Kinetic energies.

Moving into the Strong Field / High-Complexity Regime: M-Dwarf Stars

Surface magnetic field predictions from fully-convective dynamo models

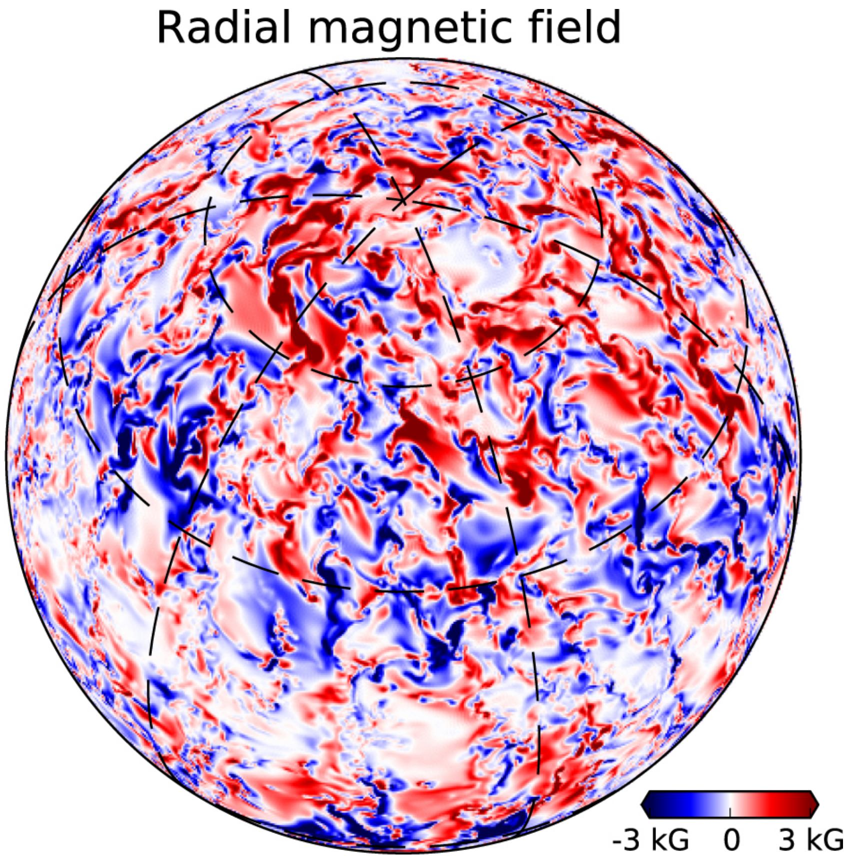

Yadav+ (2016)

Consider different CME Eruption Models (Gibson-Low / Titov-Démoulin)

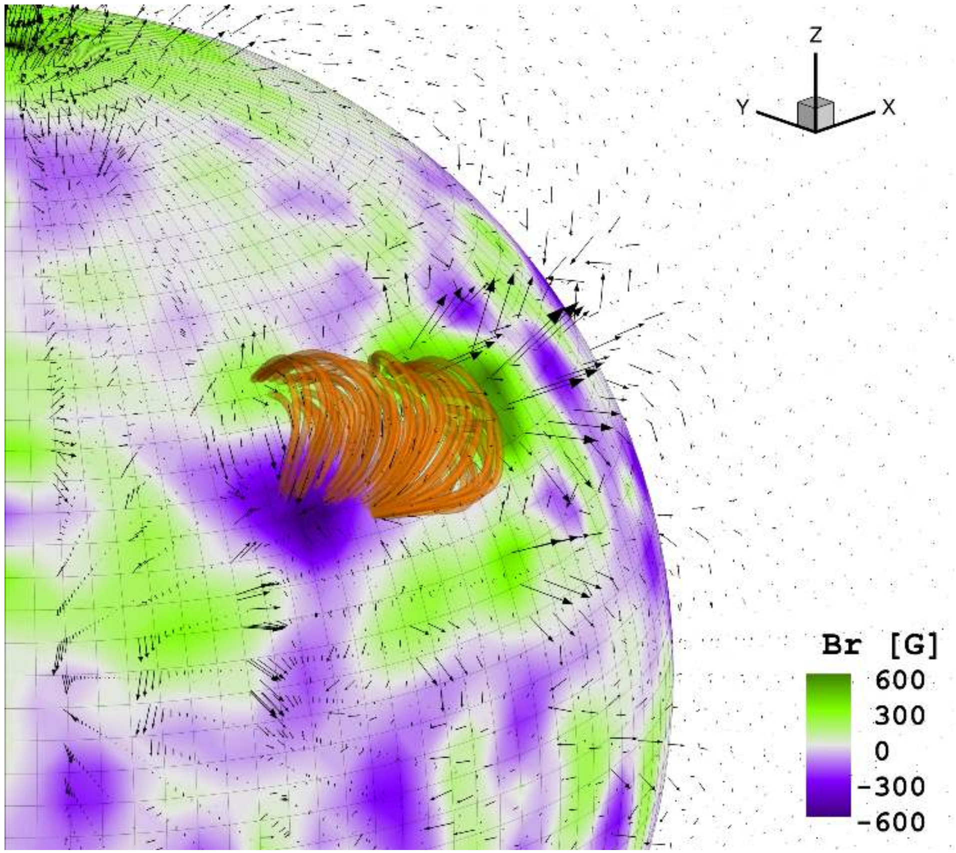

Alvarado-Gómez+ (2019b)

Coronal response after a flux-rope eruption event for different background magnetic fields (consistent with low- to moderately-active M-dwarfs; see Reiners 2014).

Exploring the CME magnetic confinement spectrum

M_{CME} ~ 4 x 10^{14} g

$E_{B\text{-}Free}$ ~ 6.5 x 10^{34} erg

Alvarado-Gómez+ (2019b)

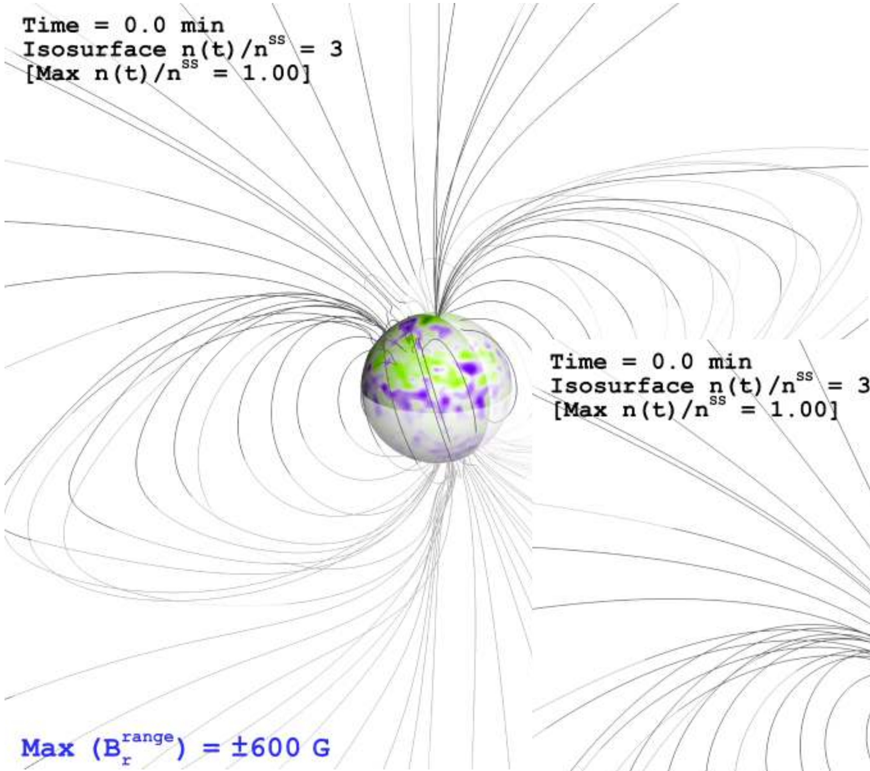

Weak

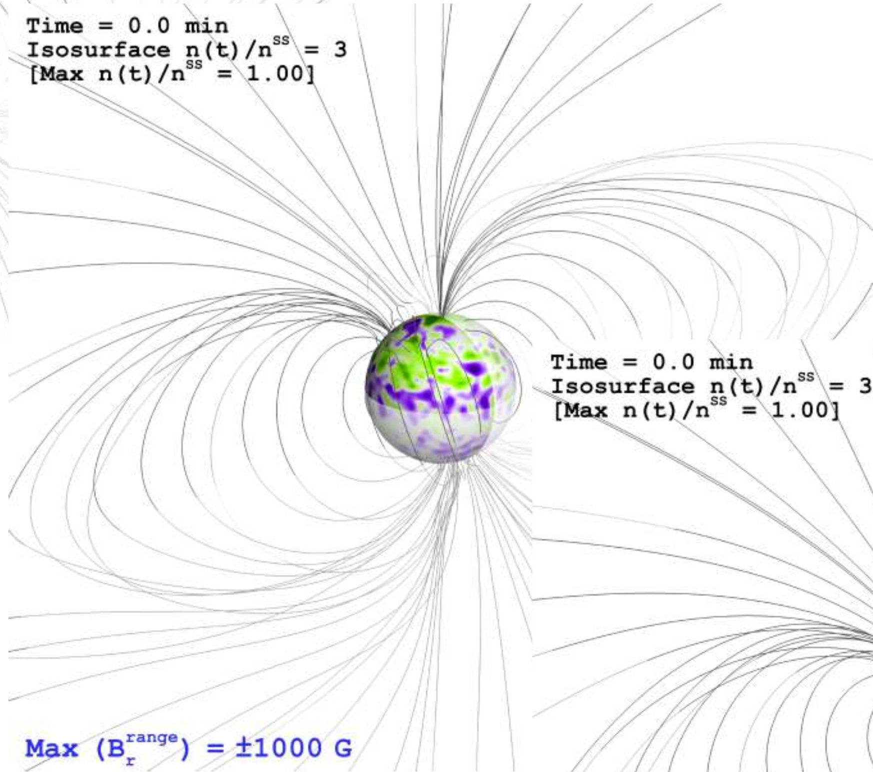

Partial

Strong

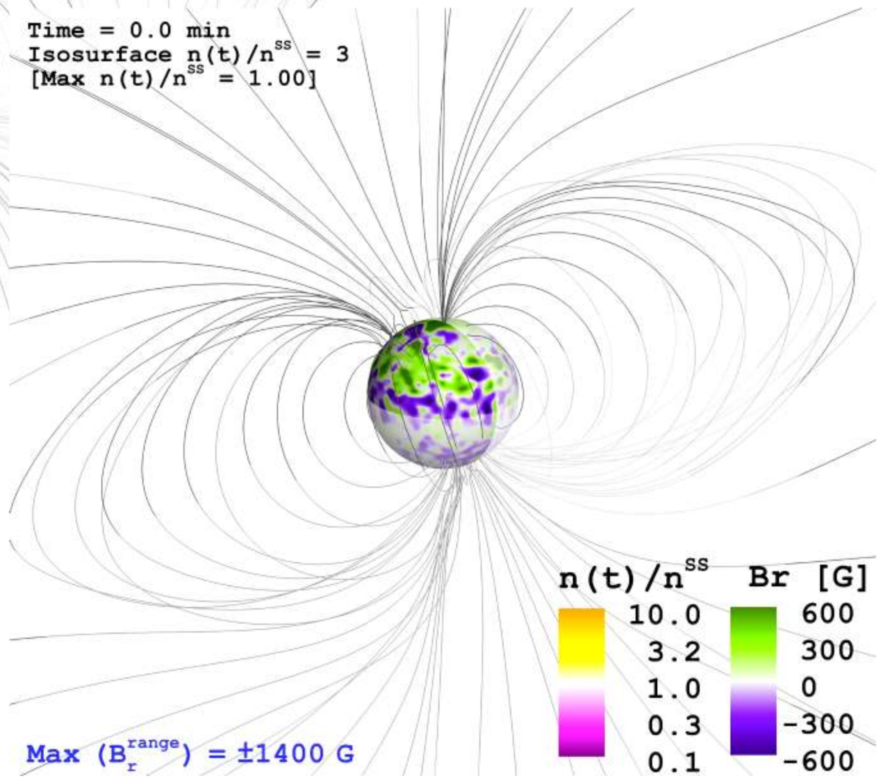

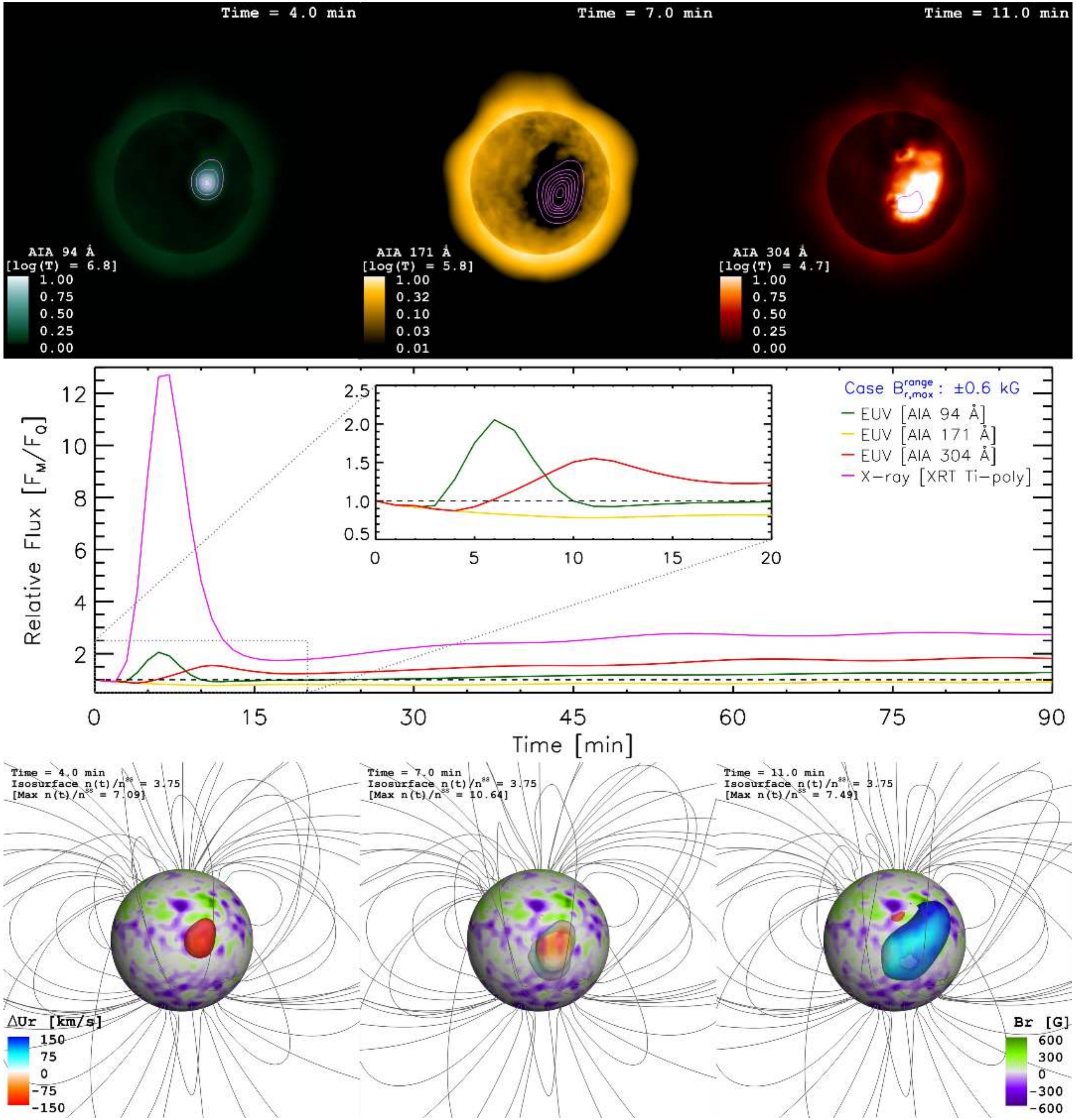

Weak CME confinement:

Collapse of the flux-rope towards the surface + `bounce' against the underlying canopy.

Induced flare-like profile (X-rays and EUV).

Transient dimming feature at mid coronal temperatures.

Distinctive progression of high-energy emission and Doppler shifts (~150 km/s).

Hints of similar processes occurring on small-scales in the Sun (Sterling+ 2015).

Partial CME confinement:

The flux-rope collapse and escape is significantly slowed down.

Longer and weaker flare-like coronal response (strong B-compression).

Longer duration coronal dimming event (mid-T).

The eruption gets disrupted. Only a small fraction escapes.

A short-lived dense prominence-like structure is formed (±100 km/s).

Signatures of coronal rain/condensations in low-T corona (±50 km/s). Similar to solar counterparts (Antolin+ 2012).

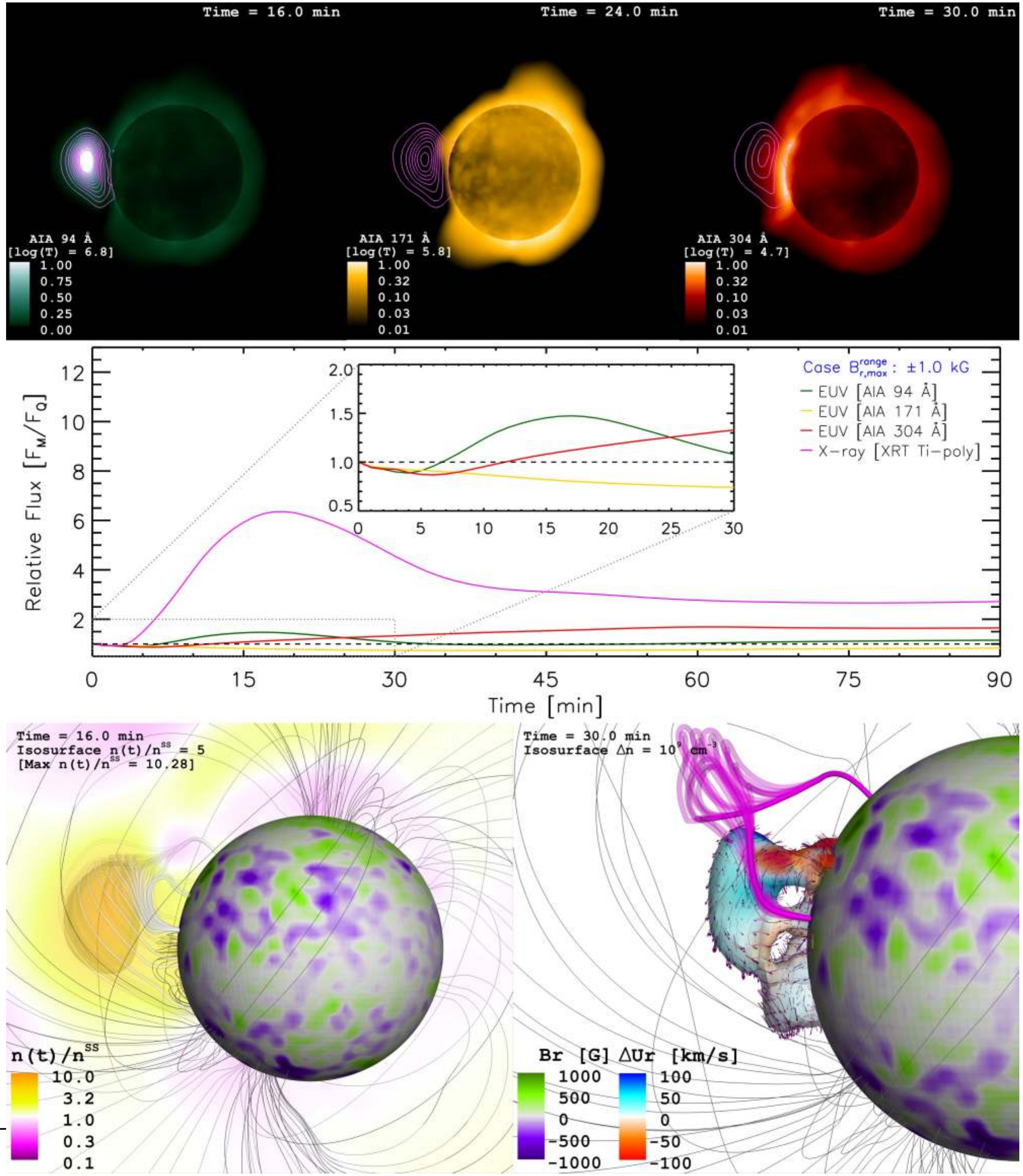

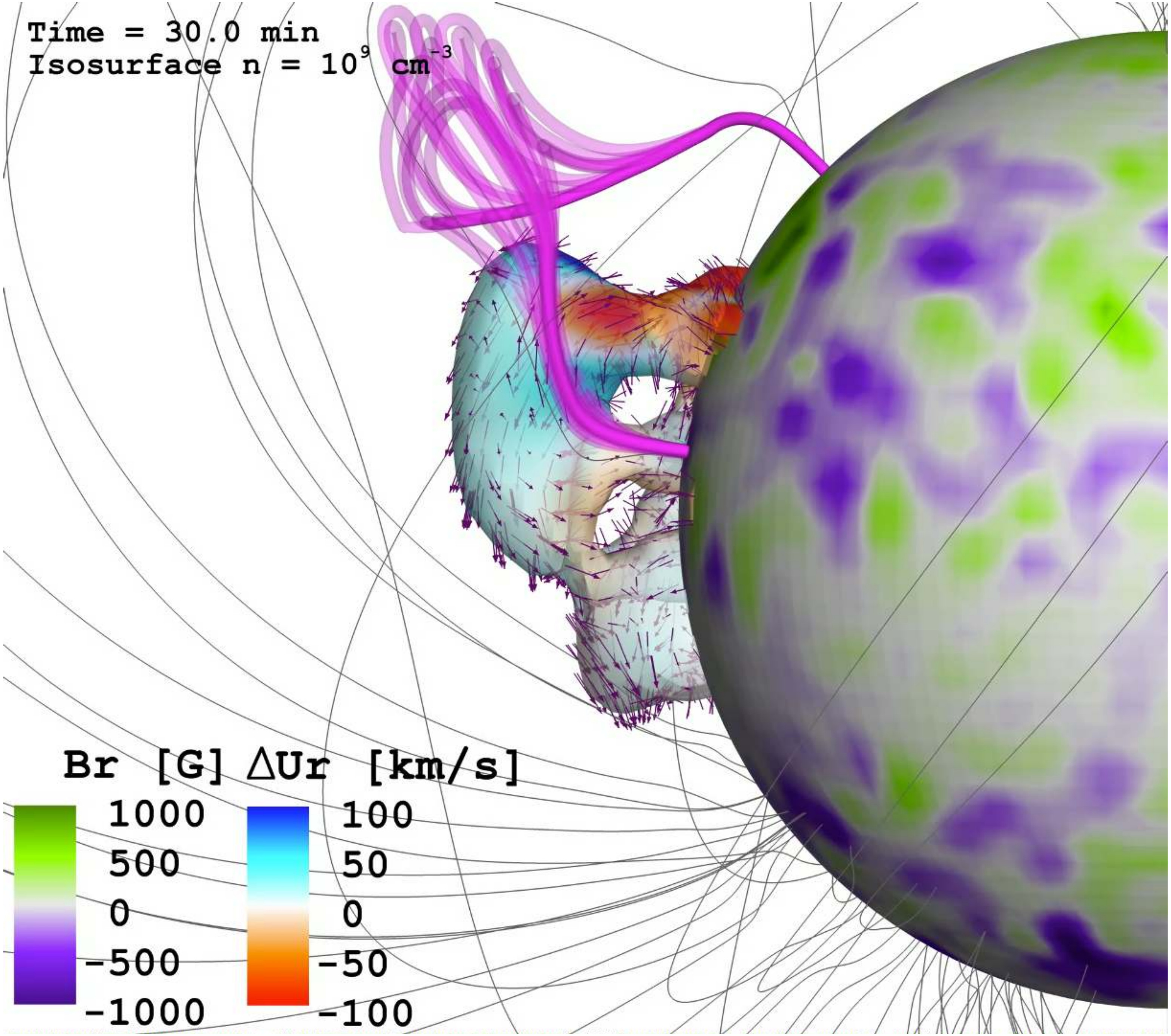
Time = 30.0 min
Isosurface n = 10^9 cm^-3
Br [G] ΔUr [km/s]
1000
500
0
-500
-1000
100
50
0
-50
-100

Stellar CME detectability based on Type-II radio bursts:

Solar radio bursts of Type II are indicative of an MHD shock in the corona/inner heliosphere, accompanied by electron acceleration. Strong connection with Solar Energetic Particle events (SEPs).

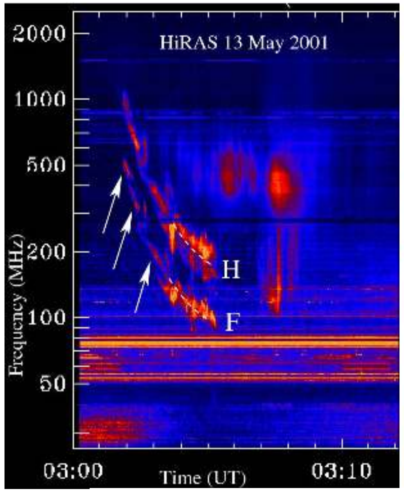

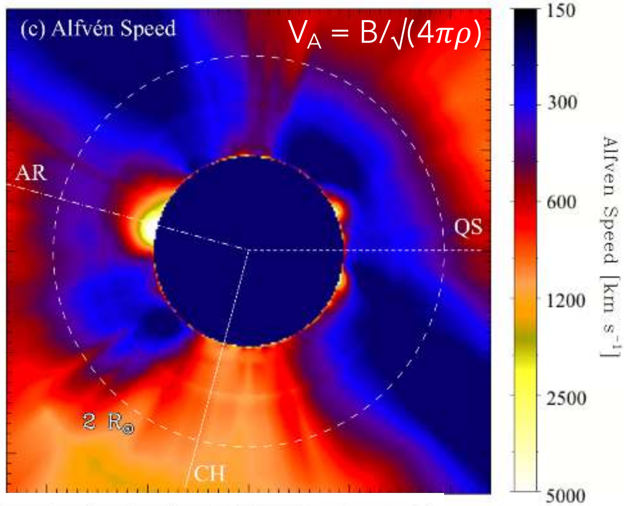

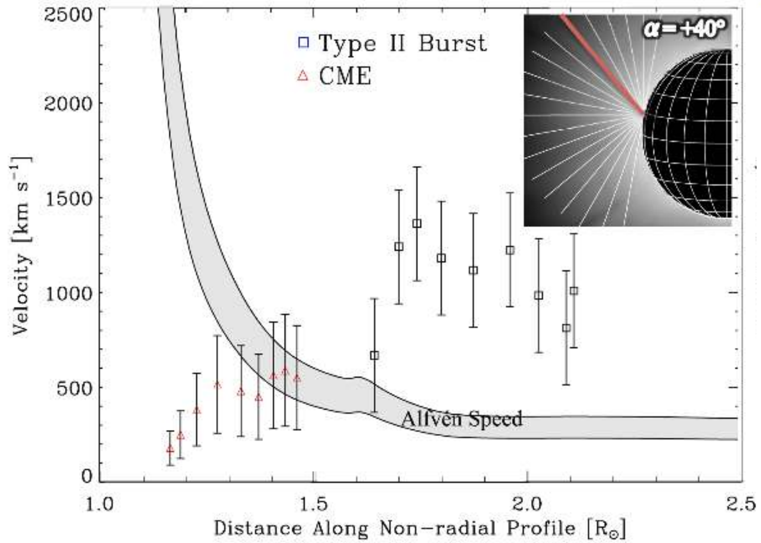

Zucca+ (2014)

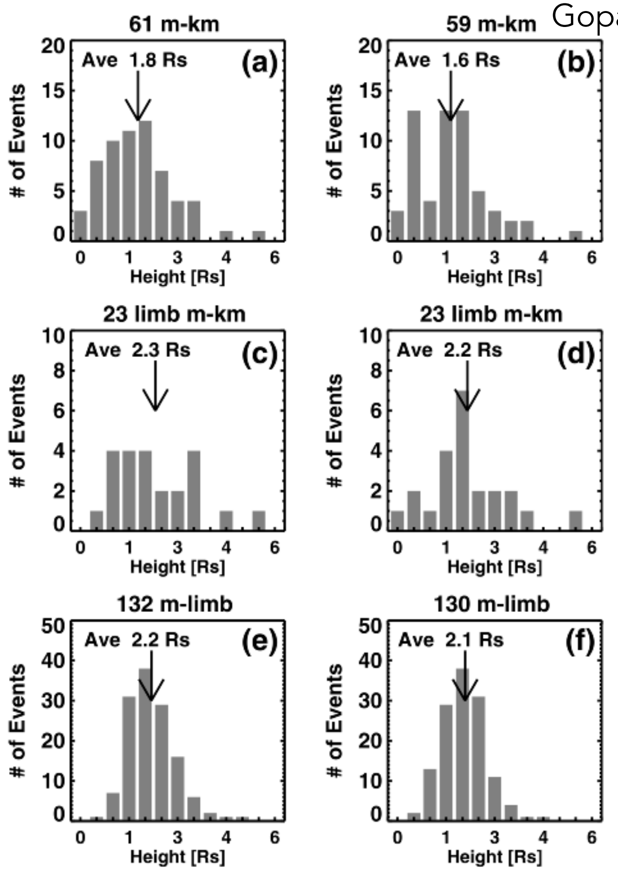

Gopalswamy+ (2005)

Shocks in solar Type II Radio bursts take place close to the surface.

The frequency (and intensity) of a type II radio burst depends on the value of the ambient density (√n).

Directionality matters: There are coronal regions more favorable for the Type II radio burst generation (e.g., astrospheric current sheet).

Alvarado-Gómez+ (2020)

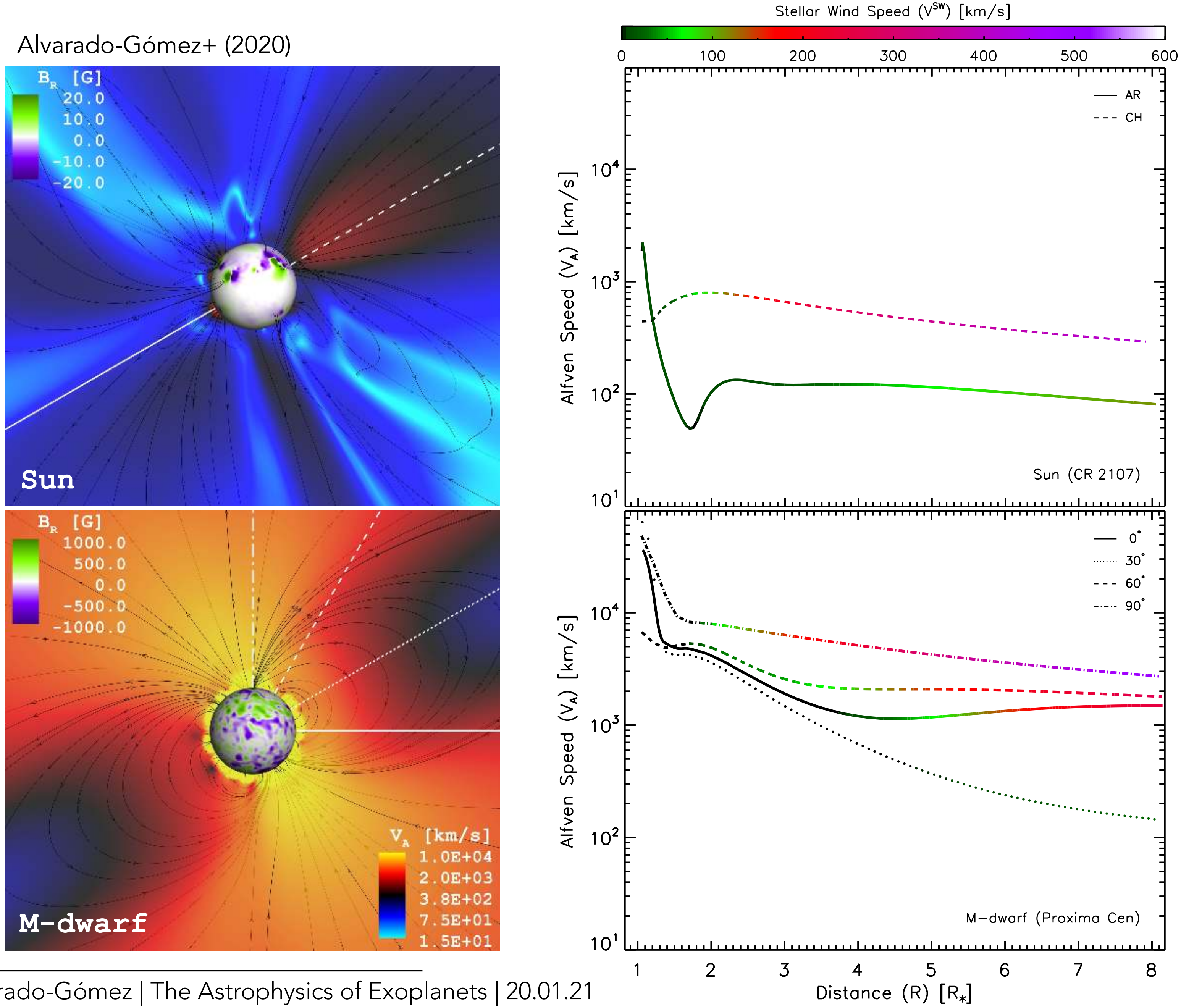

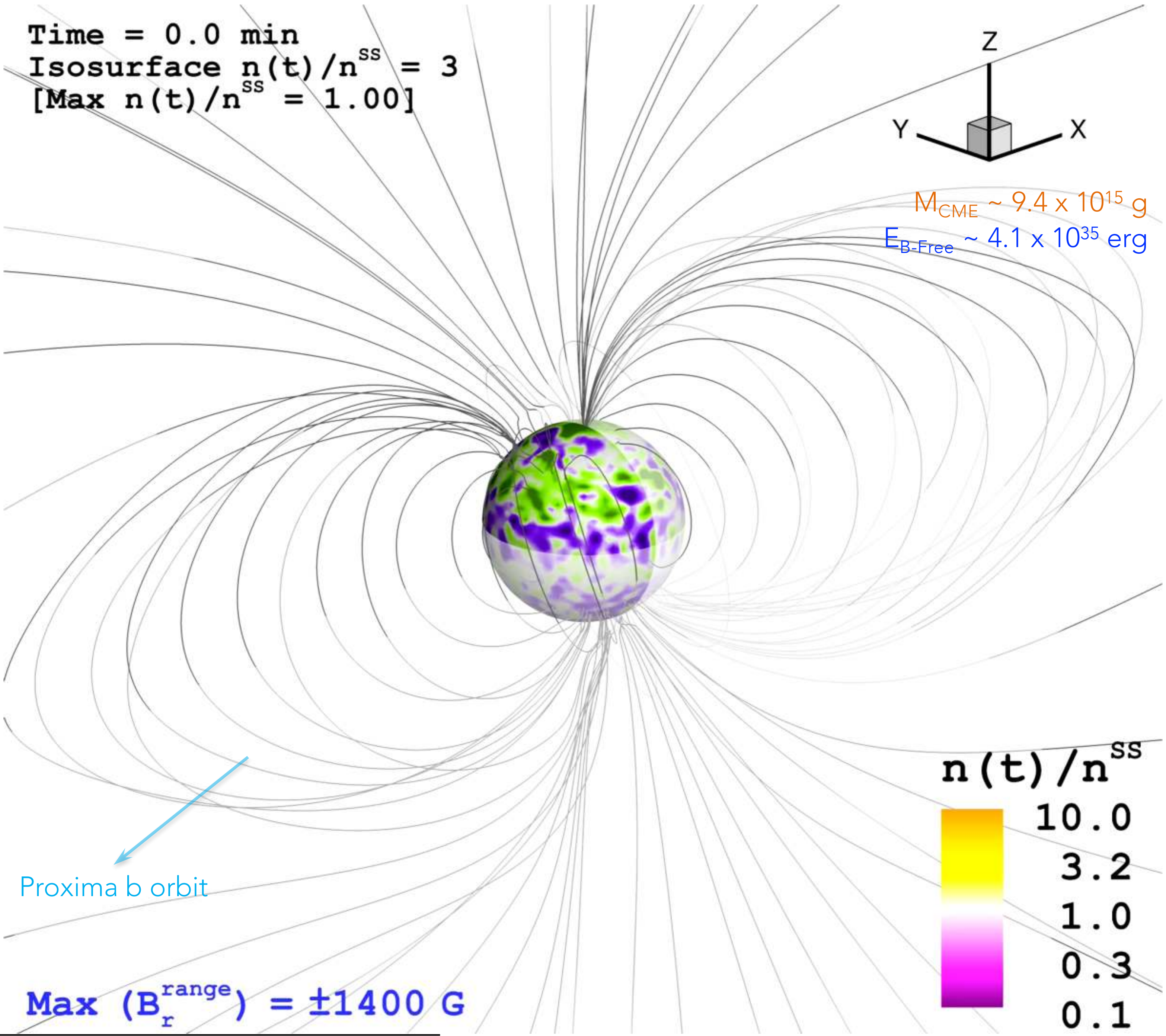

Time = 0.0 min
Isosurface n(t)/n^ss = 3
[Max n(t)/n^ss = 1.00]
Z
Y
X
M_CME ~ 9.4 x 10^15 g
E_B-Free ~ 4.1 x 10^35 erg
Proxima b orbit
Max (B_r^range) = ±1400 G
n(t)/n^ss
10.0
3.2
1.0
0.3
0.1

Due to magnetic suppression, stellar CMEs become super-Alfvénic (inducing shocks) further away from the star.

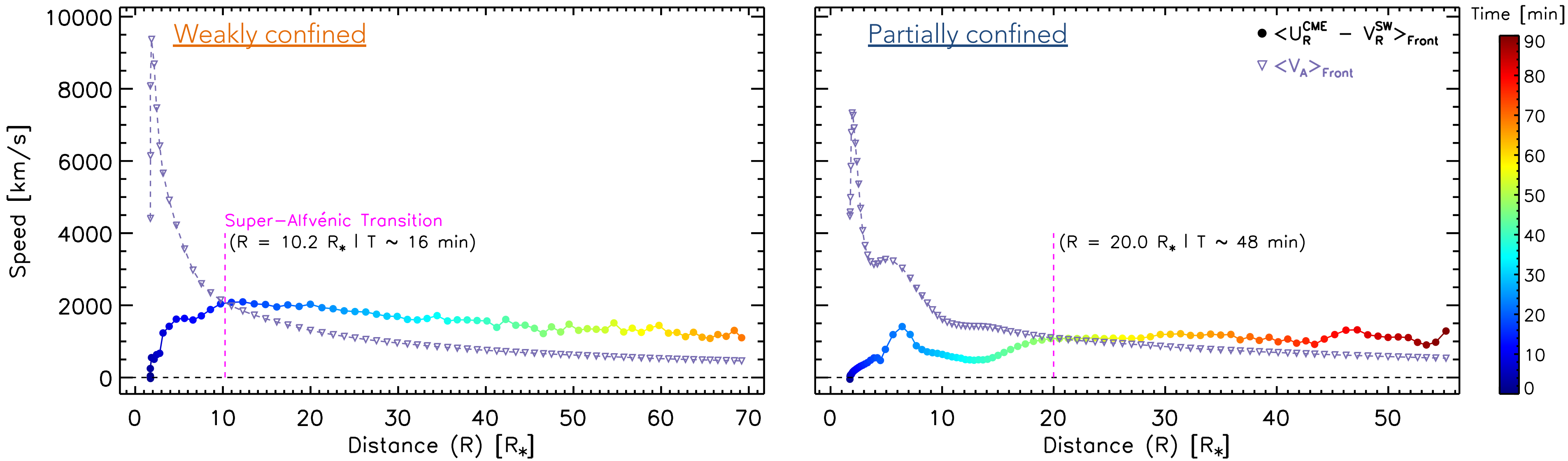

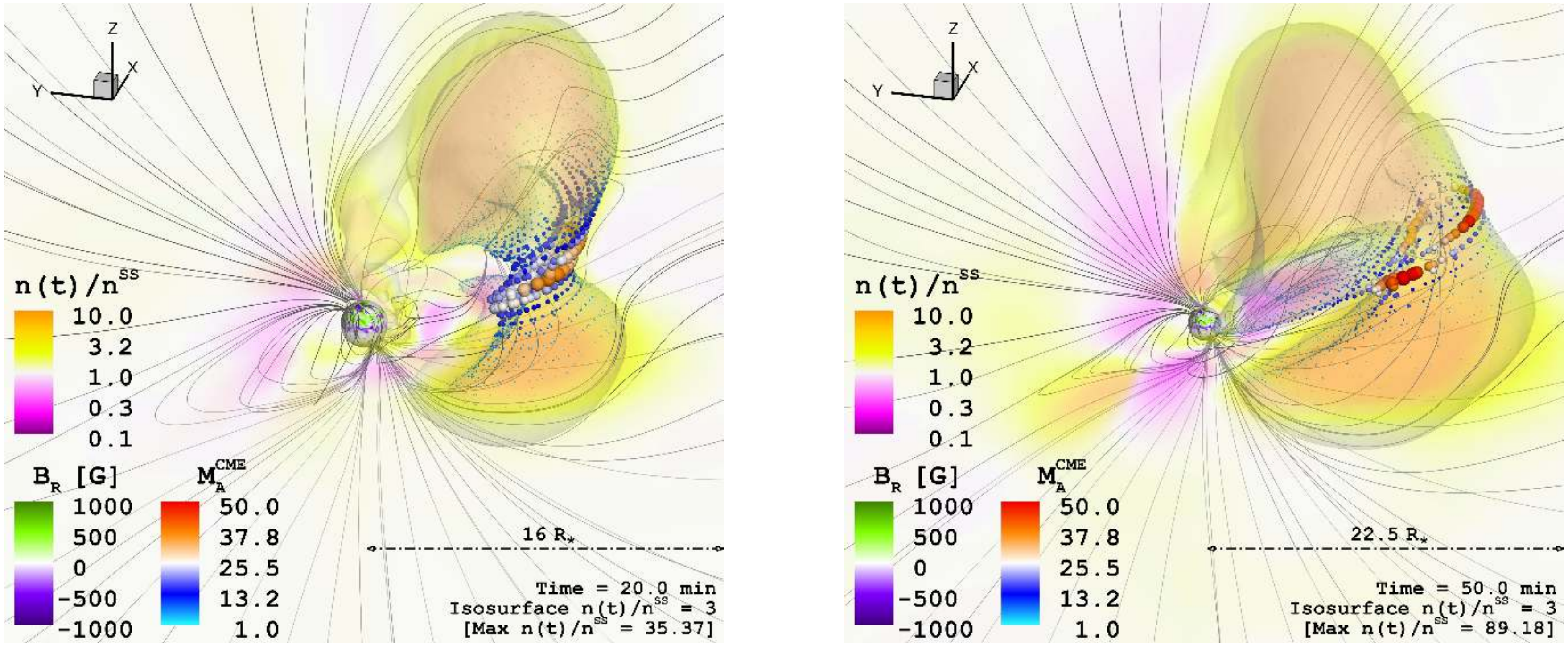

Alvarado-Gómez+ (2020)

As a consequence, the associated Type II radio bursts are shifted to larger frequencies (with lower intensities).

$\nu_p = (2\pi)^{-1} \sqrt{(4\pi e^2/m_e)} \sqrt{n} \simeq 8980 \sqrt{n}$ [Hz]

Both fundamental and harmonic lanes appear very close to the ionospheric cutoff (~10 MHz)

Not entirely ``Radio Quiet" but:

- The strongest solar type II radio bursts reach spectral fluxes up to 10^8 Jy (Schmidt & Cairns 2016).
- If occurring in Proxima: 1.4 mJy (1.3 pc)
  LOFAR sensitivity: ~5 mJy*
  SKA might reach the sensitivity but will only start at 50 MHz.

Our numerical description of Proxima Centauri provides a ``best case scenario":

- A lower bound on the mean surface field strength (~450 G, Reiners & Basri 2008).
- Highest stellar wind density allowed by observations ($\dot{M} \simeq 0.3\ \dot{M}_{\odot}$, Wood+ 2001).
- A CME shock trajectory following the current sheet (global minimum of V_A).

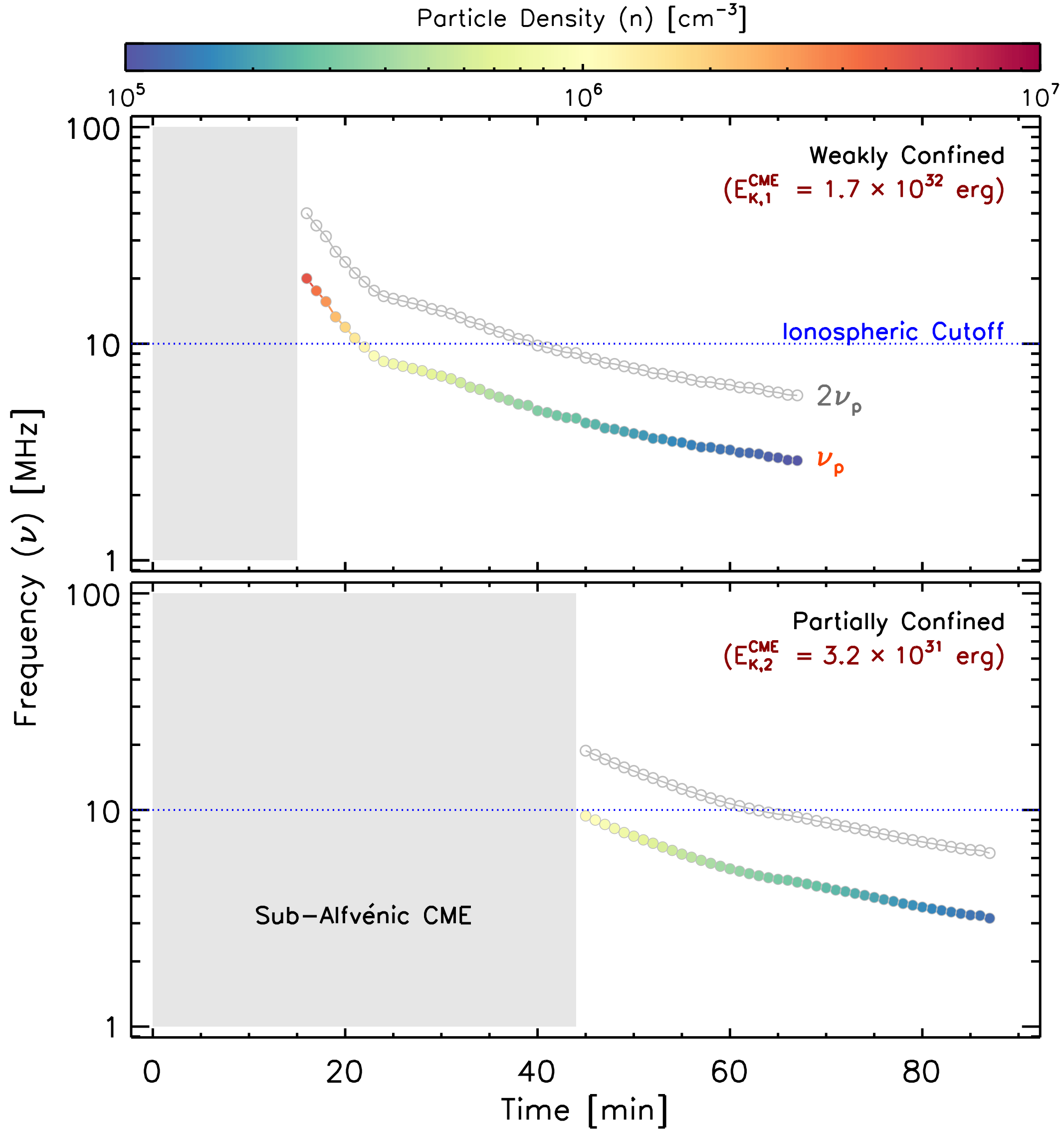

Alvarado-Gómez+ (2020)

The B-suppression of stellar CMEs greatly hampers their detectability through type II radio burst from the ground.

Concluding remarks:

- It is now possible to study in detail the properties of magnetic fields of stars other than the Sun. The wide parameter space on the stellar domain is fundamental for our understanding of how magnetism is generated on the Sun and stars.

- The study and characterization of stellar activity in any context (e.g., exoplanets) can only be complete with knowledge of its relationship with the magnetic field.

- Current exoplanet characterization efforts must include the influence due to the magnetized environment generated by the star (e.g., corona, stellar wind, flares/CMEs).

- Magnetic suppression is a viable mechanism for reducing the flare-CME association rate in active stars. The large-scale field tends to decrease the speed and energy of the CMEs. Consequences for their expected signatures and detection (e.g., "Radio quiet CMEs").

- This mechanism can be extended to a stronger / high-complexity field regime (M-dwarfs) compared to the solar case. Critical effects on the habitability around low-mass stars.

- CME confinement by the stellar large-scale magnetic field would induce additional coronal activity (e.g., flaring, up flows/down flows), possibly detectable by next-generation high-energy astrophysics instrumentation.

Thanks for your attention.